Sedimentology (2022) **69**, 2436–2462 doi: 10.1111/sed.12996

Detrital zircon in an active sedimentary recycling system: Challenging the 'source-to-sink' approach to zircon-based provenance analysis

TOM ANDERSEN*,†,[1], HERMAN VAN NIEKERK* and MARLINA A. ELBURG*
*Department of Geology, University of Johannesburg, Auckland Park, PO Box 524, 2006, Johannesburg, South Africa (E-mail: tom.andersen@nhm.uio.no)
†Department of Geosciences, University of Oslo, PO Box 1047 Blindern, N-0316, Oslo, Norway

Associate Editor – Xiumian Hu

ABSTRACT

The age and properties of detrital zircon in a sediment reflect properties of the rocks in which the zircon crystallized, and not necessarily the immediate precursor of the host sediment. Where clastic sediments are recycled, these properties are preserved so that U-Pb ages and Lu-Hf data on zircon grains will no longer give information on the routing of detritus. Because the crustal evolution and sedimentary recycling history of Southern Africa is well-established, Holocene sediments in the region provide a good test example for detrital zircon geochronology applied to sands or sandstones with a complex recycling history. Data from 16 samples of unconsolidated sand, including dunes from the southern part of the Kalahari Basin, beach sands at the Atlantic coast, and isolated inland dune occurrences, yield ranges of early Mesozoic to late Archaean ages. Uranium–lead and lutetium–hafnium isotope data provide no evidence of direct derivation of zircon from protosources in crystalline bedrock. The complex distribution patterns can be decomposed into seven 'provenance components' that have previously been encountered in Palaeoproterozoic to Jurassic sedimentary rocks in the region. These components occur in non-random combinations, in proportions that suggest mixing of recycled material from different sedimentary precursors. Taking pre-Cenozoic geology, Cretaceous to Pleistocene drainage history of southern Africa and Holocene wind and current patterns into account, it is possible to work out a consistent model for transport of detritus from sedimentary precursors into the basin, followed by aeolian remobilization within the basin itself. The detrital zircon distributions can thus be interpreted from prior knowledge of the basin filling history, regional geology, geomorphology, drainage evolution and wind pattern. This amounts to a line of reasoning from 'sink back to (intermediate) 'source', which is the opposite of the '(proto)source-to-sink' paradigm commonly invoked in detrital zircon studies.

Keywords Aeolian deposits, detrital zircon, Kalahari, Lu-Hf, sedimentary provenance, sedimentary recycling, source-to-sink, South Africa, U-Pb.

[1]Present address: Natural History Museum, University of Oslo, PO Box 1172 Blindern, N-0318, Oslo, Norway

INTRODUCTION

When a clastic sediment has been derived directly from sources in crystalline bedrock, the chemical and mineralogical composition and isotopic characteristics of the sediment can, in principle, be used to identify the sources of detritus, and to map the sedimentary transport paths. Tracing detritus 'from source to sink' is an explicit goal in many sedimentary provenance studies. It has, however, long been realized that recycling of older sediments is an important process, especially for sands and sandstones (e.g. Potter & Pryor, 1961; Blatt, 1967; Pettijohn *et al.*, 1973; Veizer & Jansen, 1979; Garzanti *et al.*, 2022). Where sedimentary recycling is important, the direct connection between original source rock and final deposit is obscured, which will influence geochemical, isotopic and mineralogical provenance indicators (e.g. Cox *et al.*, 1995; Reinhard *et al.*, 2013; Johnson *et al.*, 2018; Haile *et al.*, 2021).

Zircon has properties that has made it a popular tracer of sedimentary provenance (e.g. Fedo *et al.*, 2003; Gehrels, 2014). In its crystalline state it is physically and chemically robust, it is datable by the U-Pb method, and its Hf isotope and trace element composition reflects the rock in which it crystallized (the *protosource*). However, because of its robustness (e.g. Williams, 2001), zircon may survive repeated erosion–transport–deposition cycles. This was realized in some very early detrital zircon studies based on analysis of multi-grain fractions (Ledent *et al.*, 1964; Tatsumoto & Patterson, 1964), and has been confirmed by numerous studies based on modern, microbeam U-Pb analyses of single zircons (e.g. Røhr *et al.*, 2008, 2010; Dickinson *et al.*, 2009; Andersen *et al.*, 2011; Johnson *et al.*, 2018). The ability of zircon to survive successive recycling is, in fact, the reason why age and isotope data from detrital zircon in modern river sediments can be used to study large-scale processes of evolution of the continental crust (e.g. Belousova *et al.*, 2010; Iizuka *et al.*, 2010, 2013; Condie *et al.*, 2011).

Where sedimentary recycling is an important process, it is no longer possible to trace the transport of detritus from the protosource information given by detrital zircon data. The 'source-to-sink' paradigm, therefore cannot be applied. On this background, three questions appear to be well-justified: (i) what can we still learn from detrital zircon data; (ii) how to avoid the risk of making false geological inferences from such data; and (iii) what kind of variation in age and Hf isotope distribution patterns can be expected for detrital zircon in undisturbed sediments deposited within a relatively short time interval in a moderately sized area? In the present study, these questions are approached through a study of Quaternary sand from South Africa.

Detrital zircon U-Pb and Lu-Hf data from Palaeoproterozoic to recent sedimentary successions from southern Africa suggest that recycling of older sedimentary deposits has been an important process in the region at least since the early Neoproterozoic (Andersen *et al.*, 2016a,b, 2018a, 2019a, 2020a, 2020b; Zieger *et al.*, 2019, 2021; Gärtner *et al.*, 2021; Garzanti *et al.*, 2022). The depositional history of the sediments, the evolution of the regional drainage pattern and the wind regime at the time of deposition of Cenozoic sands are well-studied (e.g. Lancaster, 1981; Heine, 1982; Partridge & Maud, 1987; Thomas & Shaw, 1991; Bootsman, 1998; Moore, 1999; Haddon, 2005; Partridge *et al.*, 2006; Miller, 2014; Thomas & Burrough, 2016). The ages, and to some extent the Hf isotope characteristics of potential sources in crystalline basement, and sedimentary precursors in the region are relatively well-constrained by published data (Zieger *et al.*, 2019, 2021 and reviews in Andersen *et al.*, 2016b, 2018a and Zimmermann, 2018). This makes the region a useful 'natural laboratory' in which the recycling processes and their consequences can be studied in some detail. Recycling processes are, however, not restricted to southern Africa, but are potentially important for any deposit that may contain material derived from older sediments, regardless of location, age or tectonic setting.

GEOLOGICAL BACKGROUND

After breakup of the Gondwana supercontinent in the Jurassic–Cretaceous (Watkeys, 2006), the southern margin of the African continent was uplifted (Partridge *et al.*, 2006), possibly in response to mantle plume activity (Goudie, 2005). As a result, a huge depression on continental basement formed, stretching from near the equator to *ca* 29°S in the Northern Cape province of South Africa (Fig. 1), and possibly even further south-east (Partridge *et al.*, 2006; Botha, 2021). The basin was gradually filled by lacustrine, fluvial and aeolian sediments of the Cenozoic Kalahari Group (Partridge *et al.*, 2006).

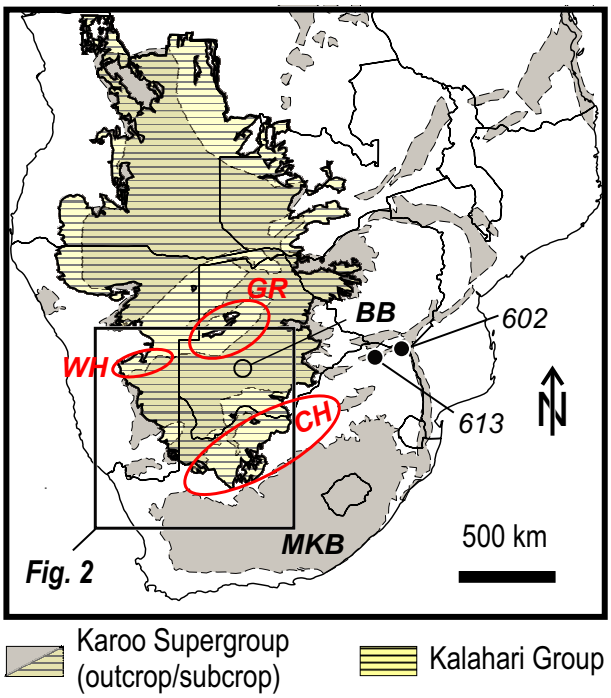

Fig. 1. Extent of the main Phanerozoic sedimentary basins in southern Africa. Late Palaeozoic–Mesozoic basins from Catuneanu *et al.* (2005), Cenozoic Kalahari Basin from Haddon (2005). MKB – Main Karoo Basin; BB – Botswana Basin (following Johnson *et al.*, 2006. This basin has also been called the 'Kalahari Basin', e.g. Catuneanu *et al.*, 2005). Basement highs are marked with red: CH – Cargonian Highlands (Visser, 1987); WH – Windhoek Highlands; GR – Ghanzi Ridge.

In southern Africa, the name 'Kalahari Basin' has been applied both to this Cenozoic basin (e.g. Thomas & Shaw, 1991), and to a Carboniferous–Cretaceous basin covering most of southern Botswana, filled by sedimentary rocks of the Karoo Supergroup (Fig. 1, e.g. Catuneanu *et al.*, 2005). To avoid confusion, this study follows Haddon (2005) and Johnson *et al.* (2006) in referring to the older basin as the 'Botswana Basin' (Fig. 1). Exposed parts of the latter basin in the east and west are known as the Ellisras Basin and Aranos Basin, respectively.

The depositional basement of the Kalahari Group in South Africa, Botswana and Namibia consists of Archaean to Palaeoproterozoic rocks of the Kaapvaal Craton and its marginal accreted Palaeoproterozoic–Mesoproterozoic terranes, the Mesoproterozoic Namaqua–Natal Belt, and sedimentary cover successions ranging in age from Neoproterozoic to Mesozoic (Catuneanu *et al.*, 2005; Cornell *et al.*, 2006; Gresse *et al.*, 2006; van Niekerk & Beukes, 2019). In much of southern and central Botswana and adjoining parts of Namibia, the Kalahari Group was deposited on Carboniferous to Mesozoic sedimentary rocks of the Karoo Supergroup of the Botswana Basin (Figs 1 to 3), which in the western part of the area rest upon Neoproterozoic to Cambrian sedimentary rocks of the Nama Group (Gresse *et al.*, 2006; Vickers-Rich *et al.*, 2016; Corner & Durrheim, 2018). North of the Ganzi Ridge in central Botswana, the Kalahari Group was deposited on rocks of the Neoproterozoic Damara Belt (Foster *et al.*, 2015), including sedimentary rocks of the Nama Group and underlying Neoproterozoic Ghanzi and Witvlei Groups (Figs 2 and 3). During deposition of the lower part of the Karoo Supergroup (Dwyka Group), the Botswana Basin was separated from the Main Karoo Basin (MKB in Fig. 1) by a broad ENE–WSW topographic high known as the Cargonian Highlands (CH in Fig. 1; Visser, 1987). In this area, the Karoo Supergroup is missing, and the Kalahari Group sediments were deposited on Precambrian basement of the Kaapvaal Craton, Kheis Terrane and Namaqua–Natal Belt (Fig. 2).

The Kalahari Group consists of a succession of conglomerates, sandstones and mudrocks deposited in fluvial and lacustrine environments, with calcrete, silcrete and ferricrete horizons, overlain by unconsolidated, aeolian sand which makes up the *Gordonia Formation* (informally known as the 'Kalahari sand'; Partridge *et al.*, 2006). A stratigraphy with six named formations, of which the Gordonia Formation is the youngest and most widely distributed, has been proposed (Fig. 3B; Partridge *et al.*, 2006). The succession below the Gordonia Formation is very poorly exposed, and the stratigraphy may not be applicable in all parts of the basin (e.g. Thomas & Shaw, 1991; Partridge *et al.*, 2006). In some areas, for example along the southern margin of the basin, only the Gordonia Formation is present.

In the southern part of the basin in south-eastern Namibia, south-western Botswana and the Northern Cape province of South Africa, the Gordonia Formation is made up by large dune fields with stable, vegetated linear dunes (e.g. Lancaster, 1981; Thomas & Shaw, 1991). Dunes may have started forming already in the Pliocene, and have remained intermittently active in the Pleistocene and Holocene (Miller, 2014; Thomas & Burrough, 2016; Stone, 2021). In the area sampled in this study, the dunes have a general north-west/south-east orientation,

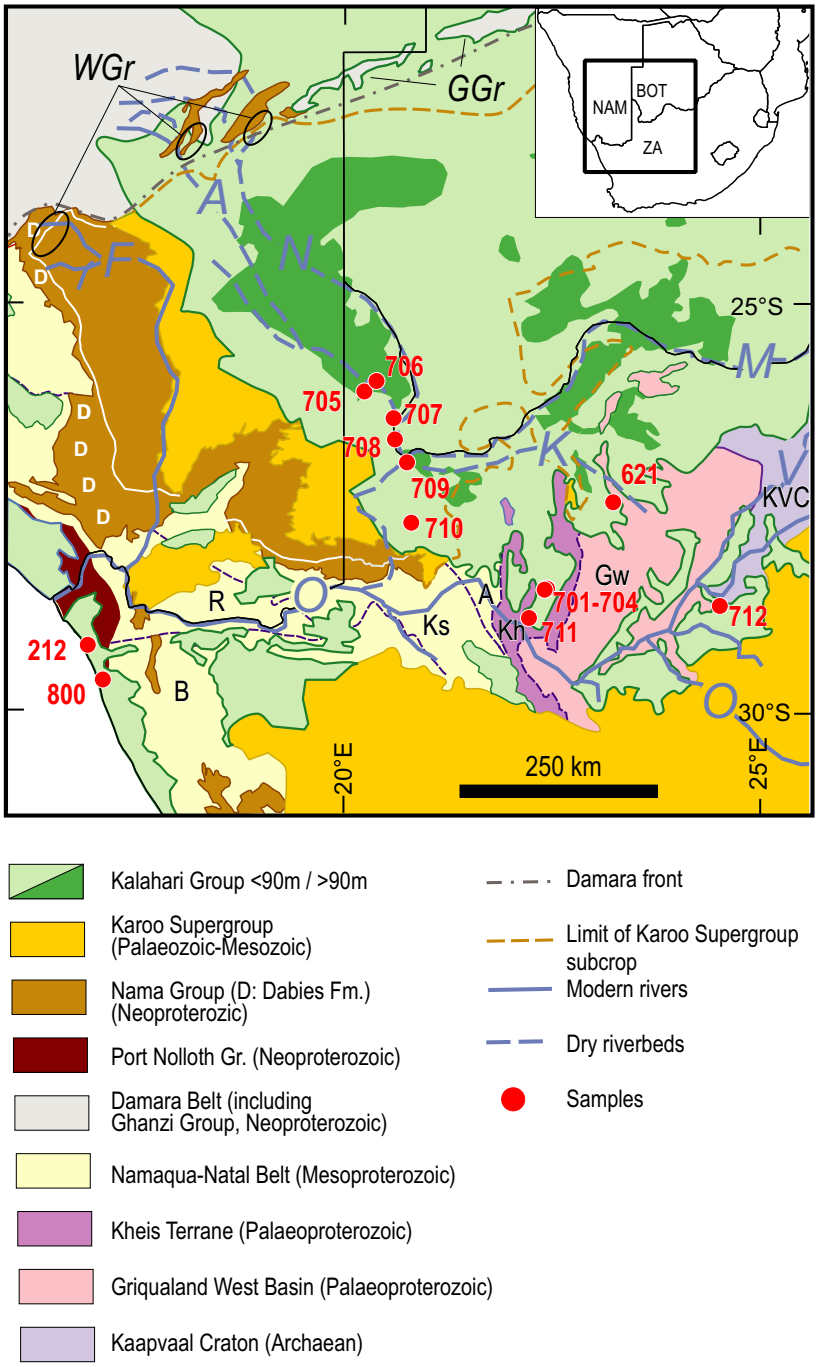

Fig. 2. Geological map showing the main features at the south-western rim of the Kalahari Basin, with localities sampled for this study. Distribution of domains in the basement from Cornell *et al.* (2006), Schlüter (2006) and van Niekerk & Beukes (2019). Late Palaeozoic–Mesozoic basins in outcrop and subcrop from Catuneanu *et al.* (2005), Kalahari Basin from Haddon (2005) and Nama Group from Vickers-Rich *et al.* (2016). The main courses of major rivers in the region are included (*O* – Orange, *V* – Vaal, *K* – Kuruman, *M* – Molopo, *N* – Nossob, *A* – Aoub, *F* – Fish River), for more details on the modern river network, see Fig. 8. Abbreviations used on the map: D – Lower part of the Nama Group (Dabis Formation, Fig. 3D), Nama Group cropping out in South Africa also mainly belongs to this Formation; KVC – Kaapvaal Craton; Gw – Griqualand West Basin (Transvaal Supergroup); Kh – Kheis Terrane (van Niekerk and Beukes, 2019); A – Areachap Terrane; Ks – Kakamas Domain; B – Bushmanland Domain; R – Richtersveld Domain; GGr – Outcrop of Neoproterozoic Ganzi Group (Hall *et al.*, 2018); WGr – Areas with outcrop of Neoproterozoic Witvlei Group, otherwise not visible on the scale of this map (Prave *et al.*, 2011).

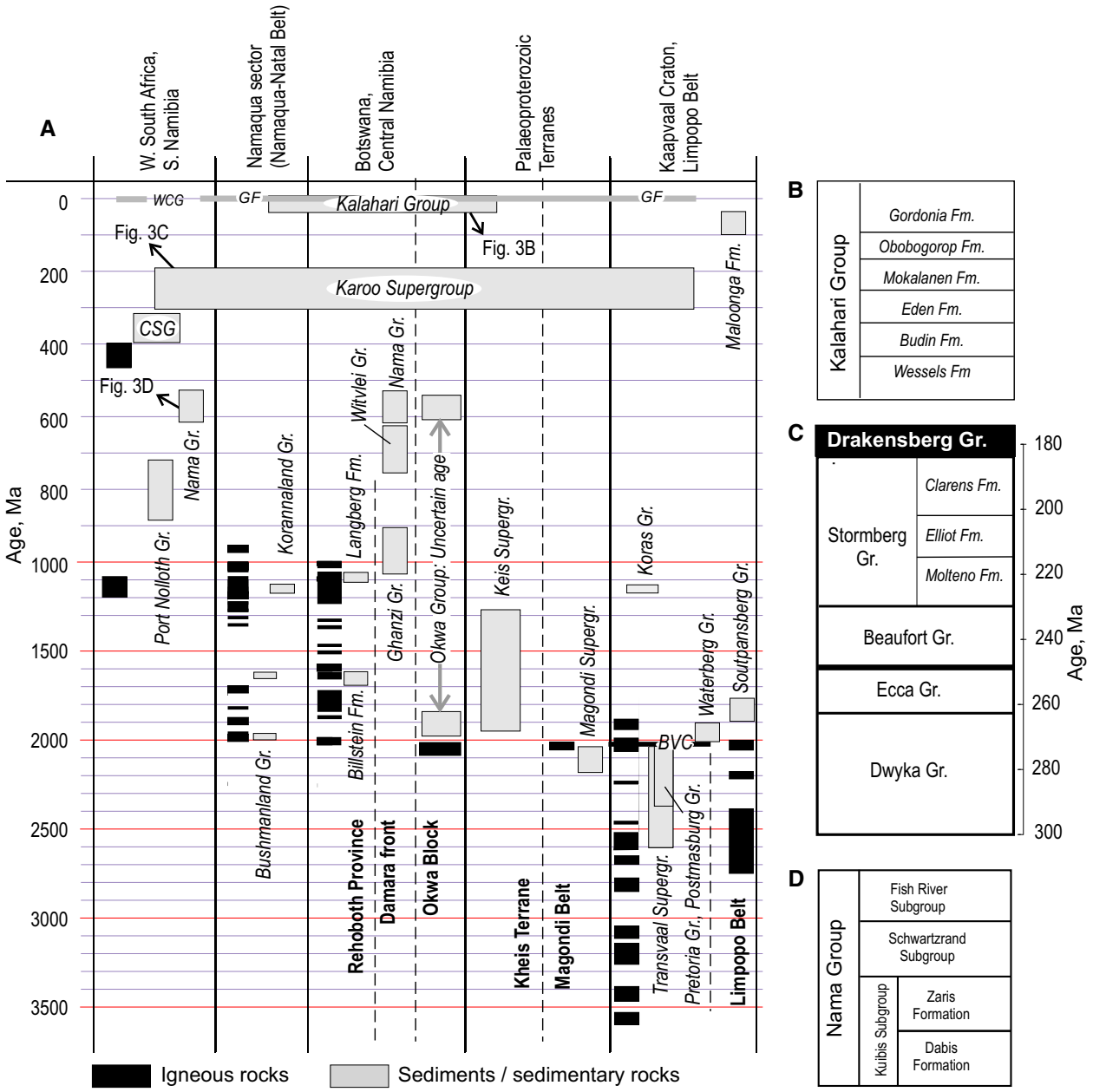

Fig. 3. (A) Simplified time-space diagram for important crustal domains in southern Africa. The timing of igneous events is based on compilation of published data in Andersen *et al.* (2018a). Abbreviations: WCG – West Coast Group (Knight, 2021); GF – Gordonia Formation; CSG – Cape Supergroup; BVC – Bushveld Complex (age from Zeh *et al.*, 2015). Sources of depositional age information for sedimentary successions: Karoo Supergroup (Johnson *et al.*, 2006), Cape Supergroup (Thamm & Johnson, 2006), Nama Group and Port Nolloth Group (Andersen *et al.*, 2018a, and references therein), Langberg and Billstein formations (van Schijndel *et al.*, 2011, 2014), Bushmanland Group (Bailie *et al.*, 2007), Korannaland Group (van Niekerk *et al.*, 2022), Ghanzi Group (Hall *et al.*, 2018), Witvlei Group (Prave *et al.*, 2011), Okwa Group (Ramokate *et al.*, 2000; Andersen *et al.*, 2020b; the depositional age of this succession is based only on detrital zircon data, and remains very uncertain), Keis Supergroup, Koras Group (van Niekerk *et al.*, 2022, and references therein), Magondi Supergroup (Master *et al.*, 2010), Transvaal Supergroup, Pretoria Group and Postmasburg Group (Eriksson *et al.*, 2006; Zeh *et al.*, 2016, 2020; Gumsley *et al.*, 2017, and references therein; Mapeo *et al.*, 2006; Moore *et al.*, 2012b), Waterberg Group (Andersen *et al.*, 2019b, and references therein), Soutpansberg Group (Andersen *et al.*, 2020a, and references therein), Malonga Formation (Botha & Wit, 1996; Andersen *et al.*, 2020a). (B) Stratigraphy of the Kalahari Group, after Partridge *et al.* (2006). (C) Simplified stratigraphy of the Karoo Supergroup, after Johnson *et al.* (2006). (D) Simplified stratigraphy of the Nama Group, after Hofmann *et al.* (2015).

whereas in the south-westernmost part of the dune field, dunes approach a WNW–ESE direction (Lancaster, 1981; Heine, 1982). Potential sources of sand in the dunes are lower stratigraphic units of the Kalahari Group, which may contain material from distal sources (Vainer *et al.*, 2018), Neoproterozoic to Phanerozoic sedimentary rocks (Nama Group and Karoo Supergroup) exposed at the western margin of the basin (Fig. 2), and Archaean to Mesoproterozoic crystalline basement rocks and their Palaeoproterozoic to Mesoproterozoic cover successions. From sediment petrography, heavy mineral assemblages and detrital zircon data on a large set of samples from different parts of the basin, Garzanti *et al.* (2022) found that the Gordonia Formation formed by extensive recycling of sediment within the basin, but with additional contributions from bedrock sources at the basin margins.

Dune and beach deposits along the Atlantic coast of South Africa belong to the Witzand (De Beer, 2010; Botha, 2021) or Swartlientjies (Browning & Roberts, 2015) Formation of the West Coast Group, or to overlying, unnamed Holocene strata (Knight, 2021). Sand drift at the west coast is generally from south to north by wave-driven longshore drift and winds from the south-west in the winter season, but with subordinate north-eastward movement (Heine, 1982; Franceschini *et al.*, 2003; Chase & Thomas, 2006; Kruger *et al.*, 2010; Roberts *et al.*, 2013; Garzanti *et al.*, 2015; Philander & Rozendaal, 2015).

ANALYTICAL METHODS AND DATA HANDLING

The sand samples analysed in this study (Table 1, Figs 1 and 2) were taken 10 to 20 cm below surface from roadcuts through dunes, in riverbeds and on natural dune surfaces. Heavy minerals were separated by manual washing in a plastic gold pan, and zircon separates were made by hand picking from the bulk heavy mineral fractions. Zircon grains were mounted in epoxy, ground to expose the grains, and polished. The zircons were imaged by cathodoluminescence (CL) in scanning electron microscopes prior to laser ablation analysis. Two instruments were used, a Hitachi SU5000 FE-SEM with Delmic Sparc-Advanced CL system (Hitachi, Tokyo, Japan) at the Department of Geosciences, University of Oslo, and a Tescan VEGA3 instrument (Tescan Orsay Holding a.s., Brno, Czech Republic) at the Spectrum Analytical Facility, University of Johannesburg.

Uranium–lead analyses were performed at the Department of Geosciences, University of Oslo, using a Bruker Aurora Elite quadrupole ICPMS (Bruker, Billerica, MA, USA) with a 213 nm CETAC LS213G2+ Nd:YAG laser microprobe (Teledyne Cetac Technologies, Omaha, NE, USA). Analytical protocols have been described by Andersen *et al.* (2016b). For Hf isotope analysis, multicollector, magnetic sector ICPMS instruments at the Department of Geosciences, University of Oslo (Nu Plasma HR with 213 nm CETAC LS213G2+ Nd:YAG laser) and Department of Geosciences, University of Johannesburg (Nu Plasma II, ASI 193 nm Excimer laser) were used. Spot sizes were 40 microns for U-Pb analysis and 50 microns for Lu-Hf ablations. Hafnium isotope analyses were made using routines and interference correction algorithms described by Elburg *et al.* (2013) and Jacobs *et al.* (2017). The decay constant of ^{176}Lu: $1.867{\cdot}10^{-11}$ a^{-1} of Söderlund *et al.* (2004) was used, and the Lu-Hf parameters of chondritic uniform reservoir (CHUR) and depleted mantle (DM) models were: present-day $^{176}Hf/^{177}Hf_{CHUR}$ = 0.282785, $^{176}Lu/^{177}Hf_{CHUR}$ = 0.0336 (Bouvier *et al.*, 2008), present-day $^{176}Hf/^{177}Hf_{DM}$ = 0.28325, $^{176}Lu/^{177}Hf_{DM}$ = 0.0388 (Griffin *et al.*, 2000, modified to the CHUR composition and decay constant used in this study). The Lu-Hf model ages relative to depleted mantle were calculated as part of the pairwise comparison procedure (below). Because model ages are used only for fingerprinting and comparison purposes, their use in this procedure is not influenced by the history of the crustal protolith; in fact, any model would work equally well, as long as it is applied consistently.

Concentrations of U and Th were recorded during U-Pb ablation, and raw data reduced using GLITTER software (Griffin *et al.*, 2008) with NIST-SRM 610 as calibration standard and ^{29}Si as internal standard. Uranium and Th concentrations in samples 703, 704, 705 and 706 were determined in separate analytical sessions, using the Bruker Aurora Elite instrument and standardization as above.

The most precise of the $^{207}Pb/^{206}Pb$ and $^{206}Pb/^{238}U$ ages were used to construct age distribution curves. In general, this would be the $^{207}Pb/^{206}Pb$ age for Archaean to late Mesoproterozoic grains, and the $^{206}Pb/^{238}U$ age for grains

Table 1. Samples analysed in this study.

Sample	Decimal degrees E	Decimal degrees S	Geomorphic province*	Description	Deposited on	Number of grains†
Kalahari Group						
621	23.303	27.507	Lower Vaal and Orange valleys	Dune sand	Transvaal Supergroup	95/76/29
701	22.493	28.560	Lower Vaal and Orange valleys	Dune sand	Keis Supergroup	90/63/81
702	22.493	28.566	Lower Vaal and Orange valleys	Dune sand	Keis Supergroup	88/66/73
703	22.463	28.578	Lower Vaal and Orange valleys	Dune sand	Keis Supergroup	68/57/67
704	22.463	28.578	Lower Vaal and Orange valleys	Dune sand	Keis Supergroup	93/75/93
705	20.256	26.150	Southern Kalahari	Dune sand	Kalahari Group	47/37/30
706	20.405	26.022	Southern Kalahari	Sand in dry river bed	Kalahari Group	87/67/76
707	20.613	26.478	Southern Kalahari	Sand in dry river bed	Kalahari Group	80/68/74
708	20.630	26.738	Southern Kalahari	Dune sand	Kalahari Group	80/67/70
709	20.778	27.019	Lower Vaal and Orange valleys	Dune sand	Kalahari Group	98/86/80
710	20.830	27.758	Lower Vaal and Orange valleys	Dune sand	Kalahari Group	99/89/30
711	22.272	28.925	Lower Vaal and Orange valleys	Dune sand	Keis Supergroup	93/84/31
712	24.609	28.778	Southern Highveld	Dune sand	Kaapvaal Craton	86/81/29
Atlantic Coast						
212	16.868	29.254	Namib	Beach sand	Port Nolloth Group, Gariep Supergroup	87/65/29
800	17.087	29.680	Namib	Beach sand	Port Nolloth Group, Gariep Supergroup	96/61/32
Isolated dunes						
602	30.948	22.434	Soutpansberg	Dune sand	Clarens Formation, Karoo Supergroup	100/94/28
613	29.642	22.854	Soutpansberg	Dune sand	Wylliespoort Formation, Soutpansberg Group	98/87/27

* Geomorphic provinces after Botha (2021).
† Given as $N_{\text{Total U-Pb}}/N_{\text{Useful U-Pb}}/N_{\text{Hf}}$.

that are younger. The actual switch-over point between the two depends on the respective relative precisions. Zircon grains were corrected for common lead where necessary, using a conventional ^{204}Pb correction with a composition of common lead according to the Stacey & Kramers (1975) model at the ^{206}Pb/^{238}U age of the zircon. Correction for common lead is a potential source of U-Pb age bias (Andersen *et al.*, 2019a). Therefore, analyses of Neoproterozoic and older grains that were corrected for more than 0.2% common ^{206}Pb were not used to construct distribution curves (Andersen *et al.*, 2019b; Andersen & Elburg, 2022). However, because the ^{206}Pb/^{238}U age for Palaeozoic grains is relatively robust against common lead contamination (Andersen, 2002; Andersen *et al.*, 2019a), uncorrected ^{206}Pb/^{238}U ages were used for these, regardless of their ^{206}Pb/^{204}Pb ratio.

Analyses of all unknowns are given in Table S1, including data for grains that were rejected because of elevated common lead content, and pre-correction values for analyses that were corrected for common lead. Reference zircons of known age and composition were analysed regularly during the laboratory sessions, results for these are summarized in Table 2.

Table 2. U-Pb and Lu-Hf isotope data for reference samples run as unknowns. *N*, number of analyses. References: 1 – Woodhead & Hergt (2005); 2 – Heinonen *et al.* (2010); 3 – Heilimo *et al.* (2011); 4 – Andersen *et al.* (2019a).

Reference sample	*N*	$^{176}Hf/^{177}Hf$	2SD	$^{178}Hf/^{177}Hf$	2SD	$^{176}Lu/^{177}Hf$	2SD	$^{176}Yb/^{177}Hf$	2SD	Age (Ma)	2SD	$^{176}Hf/^{177}Hf(t)$	$\varepsilon_{HF}(t)$	Reference
Oslo														
STA	67									291*	2			
A44	71									2719†	4			
LV11	19	0.28283	6	1.46720	10	0.003	2	0.21	13	290		0.28281	7.5	
MT	90	0.28249	3	1.46724	8	0.00004	2	0.0021	13	730		0.28249	5.9	
Johannesburg														
LV11	20	0.28281	4	1.46714	9	0.0027	10	0.12	40	290		0.28280	7.0	
MT	28	0.28250	5	1.46713	12	0.00003	1	0.001	2	730		0.28250	6.2	
TEM	20	0.28267	2	1.46716	8	0.0014	8	0.04	2	417		0.28266	4.8	
Published values														
LV11		0.282830	28											2
MT		0.282507	6											1
TEM		0.282686	8											1
A44										2722	4			3
STA										294.2	0.3			4

* Weighted average $^{206}Pb/^{238}U$ age.† Weighted average $^{207}Pb/^{206}Pb$ age.

Pairwise comparison of U-Pb age and Lu-Hf model age distributions were done by evaluating the degree of overlap, denoted O ($0 < O \leq 1$) of the 95% confidence bands associated with the cumulative distributions (Andersen *et al.*, 2016b, 2018b): $1\text{-}O$ is a robust measure of difference between two cumulative distributions. Overlap over the full probability domain of two distributions ($1\text{-}O = 0$) indicates that the two distributions are formally indistinguishable within error.

RESULTS

Shape and zoning of detrital zircon grains

The shape of zircon grains (Fig. 4) in the sands varies from equidimensional and well-rounded (Fig. 4C and D) through various degrees of sub-rounded, short prisms to elongated prismatic with sharp edges; the latter are most frequent in grains of Palaeozoic age (Fig. 4J to L). Well-preserved short wavelength – low amplitude oscillatory zoning, characteristic of magmatic zircon, is present in both angular (Fig. 4I) and rounded grains (Fig. 4A, F and I). Some oscillatory zoned grains have been broken along fractures whose surfaces were abraded before final deposition (Fig. 4A, B and F). Oscillatory zoning patterns are overprinted by CL bright patches and embayments (Fig. 4B and K), and cut by fractures associated with reduced CL brightness (Fig. 4D). Some grains have irregular CL patterns or are completely structureless (Fig. 4C). In general, overprinting or disturbance of the CL structure is more frequent and more pronounced in Archaean (Fig. 4B and C) than in younger grains, but even Palaeozoic grains may show disturbed CL patterns (Fig. 4K). Cathodoluminescence-bright rims occur relatively frequently; such rims may have formed before final abrasion of the grain (Fig. 4I), or after (Fig. 4E, G and H), i.e. by *in situ* alteration after final deposition (Andersen & Elburg, 2022).

Uranium–lead age distributions

Detrital zircon ages in the samples range from late Palaeozoic to Archaean (Table S1). Pairwise comparison of the U-Pb age and Lu-Hf depleted mantle model age distributions based on overlap of the confidence bands of the cumulative distribution curves suggests that the suite of samples can be divided into five groups of internally indistinguishable samples (Fig. 5).

Cumulative age distribution curves for detrital zircon in the samples of this study are shown in Fig. 6 and compared to published age distributions from older sedimentary rocks and unconsolidated, young sediments in the region (*c.f.* Fig. 3).

Samples *621, 701, 702, 703* and *704* come from an area with discontinuous dune cover on a depositional basement of metasedimentary rocks of the Palaeoproterozoic Transvaal Supergroup (621), and sandstones and quartzites of the Keis Supergroup (701 to 704). These samples have major age fractions in the range 2000 to 2150 Ma and between 900 and 1100 Ma, accompanied by a minor amount of zircon with ages between 1100 and 1300 Ma (Fig. 6A). In addition, there is a range of zircon ages between 2400 and 2800 Ma, but without any sharply defined frequency maxima in this range, and a minor but well-defined late Neoproterozoic to Cambrian (500 to 750 Ma) age fraction.

A combination of early Neoproterozoic and late Neoproterozoic–Cambrian zircon age fractions is characteristic for both the Zaris Formation and higher stratigraphic units of the Neoproterozoic Nama Group, and the lower part of the Karoo Supergroup (Blanco *et al.*, 2011; Hofmann *et al.*, 2015; Andersen *et al.*, 2016b, 2018a; Zieger *et al.*, 2019). The older, Palaeoproterozoic to Archaean zircon fractions in these samples strongly resemble the age distribution reported from the Palaeoproterozoic Waterberg Group in north-eastern South Africa (Andersen *et al.*, 2019a); similar age distributions have been reported from sandstones of the Keis Supergroup by da Silva (2011), Dreyer (2014) and van Niekerk *et al.* (2022). Proterozoic sandstones with similar Palaeoproterozoic – Archaean detrital zircon distribution patterns may have a wider distribution in Botswana, but mainly occur in subcrop covered by Phanerozoic deposits (Mapeo *et al.*, 2004; Andersen *et al.*, 2020b).

Samples *705*, *706* and *707* are from a dune (705) and from windblown sand in the dry Auob riverbed upstream (706) and downstream (707) from the confluence with the dry Nossob river (Fig. 2). These samples are all from an area with thick (>90 m) deposits of the Kalahari Group (Fig. 2, isopach contour from Haddon, 2005). The samples have indistinguishable age distribution patterns (Fig. 5), characterized by a major fraction of zircon in the 900 to 1300 Ma age range, and minor fractions at 1750 to 1975 Ma and in the Neoproterozoic (<750 Ma) to

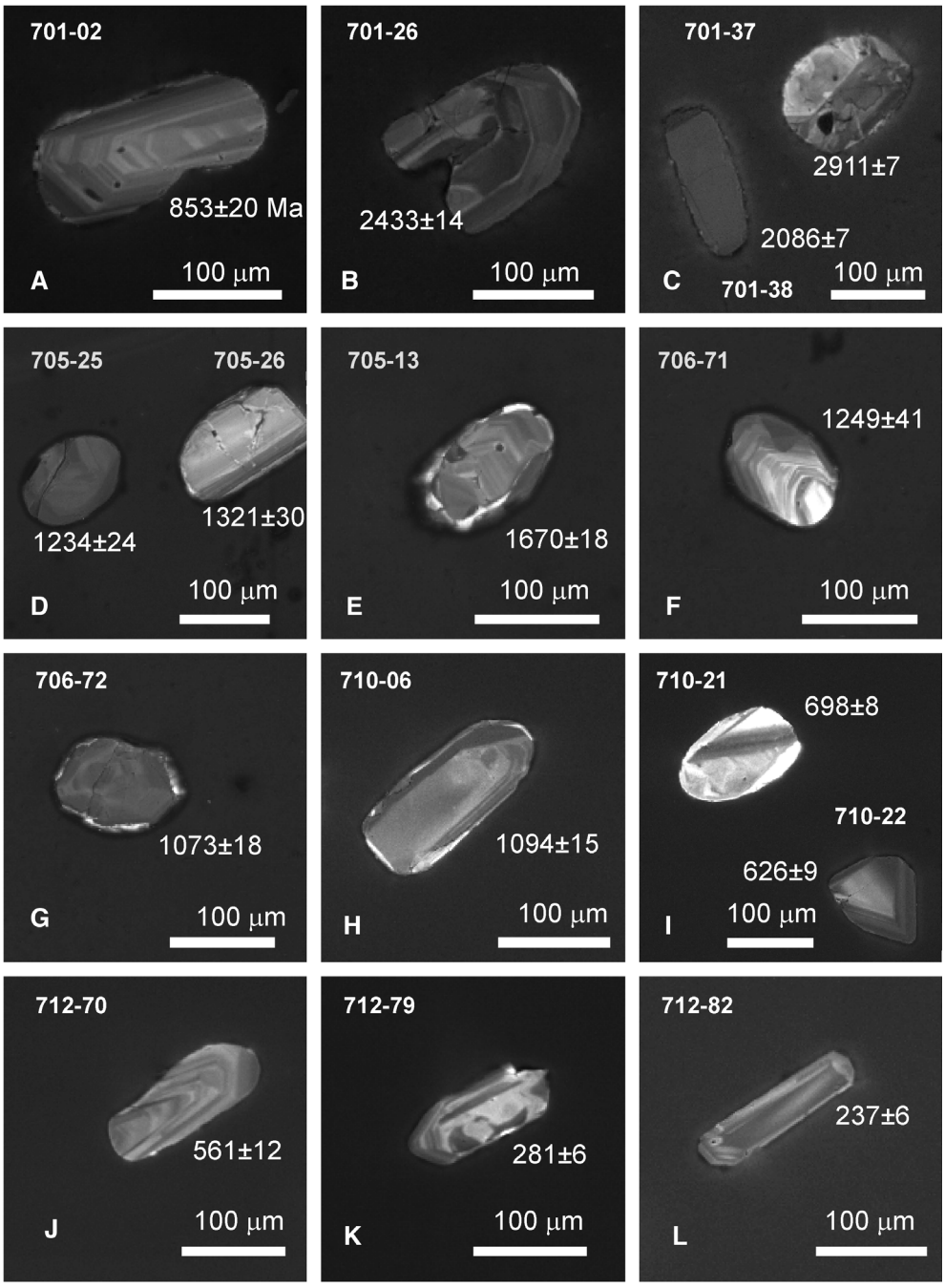

Fig. 4. Representative examples of morphology and internal structure of zircon grains in the sand samples. Grains are identified by analysis numbers in the Supplementary Table, and the age of each grain is given. See further discussion of the features in the text.

Cambrian (Fig. 6B). Similar age distributions were reported by Garzanti *et al.* (2022) from the Gordonia Formation in the Nossob river valley (their Nossob Basin, Fig. 6B). The combination of 1775 to 1950 Ma and 1100 to 1300 Ma zircon resembles age distributions reported from sandstones of Early Neoproterozoic age in the Ghanzi Group, Botswana (Hall *et al.*, 2018), Witvlei Group in central Namibia (Hofmann *et al.*, 2015), the Port Nolloth Group of the Gariep Belt, and the Dabis Formation of the Nama Group (Andersen *et al.*, 2018a). Zircon younger

	SA18-621	SA19-701	SA19-702	SA19-703	SA19-704	SA19-705	SA19-706	SA19-707	SA19-708	SA19-709	SA10-710	SA19-711	SA19-712	SA18-602	SA18-613	SA14-212	KLZ-800
	U-Pb age distributions																
SA18-621		0.00	0.00	0.00	0.00	0.00	0.00	0.00	0.00	0.00	0.00	0.00	0.13	0.10	0.02	0.00	0.00
SA19-701	0.00		0.00	0.00	0.00	0.00	0.00	0.02	0.01	0.00	0.03	0.00	0.33	0.13	0.04	0.02	0.00
SA19-702	0.00	0.00		0.00	0.00	0.00	0.00	0.06	0.21	0.02	0.21	0.00	0.38	0.40	0.12	0.05	0.06
SA19-703	0.00	0.00	0.00		0.00	0.05	0.06	0.08	0.26	0.24	0.26	0.24	0.40	0.39	0.16	0.22	0.21
SA19-704	0.00	0.00	0.00	0.00		0.07	0.07	0.08	0.23	0.22	0.26	0.24	0.39	0.38	0.16	0.22	0.22
SA19-705	0.00	0.00	0.00	0.00	0.00		0.00	0.00	0.00	0.00	0.00	0.00	0.15	0.13	0.11	0.00	0.00
SA19-706	0.00	0.00	0.00	0.00	0.00	0.00		0.00	0.06	0.03	0.06	0.07	0.20	0.18	0.13	0.00	0.00
SA19-707	0.00	0.00	0.07	0.00	0.06	0.00	0.00		0.07	0.03	0.07	0.06	0.24	0.20	0.14	0.00	0.00
SA19-708	0.00	0.01	0.16	0.08	0.26	0.02	0.10	0.01		0.00	0.00	0.00	0.10	0.01	0.00	0.00	0.00
SA19-709	0.00	0.00	0.00	0.00	0.00	0.00	0.00	0.00	0.00		0.00	0.00	0.12	0.09	0.00	0.00	0.00
SA10-710	0.00	0.00	0.07	0.02	0.13	0.00	0.09	0.00	0.00	0.00		0.00	0.13	0.06	0.02	0.00	0.00
SA19-711	0.00	0.00	0.00	0.01	0.00	0.00	0.10	0.00	0.00	0.00	0.00		0.06	0.01	0.00	0.01	0.00
SA19-712	0.00	0.08	0.17	0.22	0.29	0.13	0.14	0.14	0.00	0.00	0.00	0.00		0.00	0.00	0.16	0.15
SA18-602	0.00	0.00	0.06	0.13	0.20	0.00	0.11	0.01	0.00	0.00	0.00	0.00	0.00		0.00	0.13	0.13
SA18-613	0.00	0.00	0.00	0.00	0.00	0.00	0.04	0.00	0.00	0.00	0.00	0.00	0.00	0.00		0.11	0.12
SA14-212	0.00	0.00	0.00	0.00	0.01	0.00	0.00	0.00	0.00	0.00	0.00	0.00	0.02	0.00	0.00		0.00
KLZ-800	0.00	0.00	0.04	0.00	0.06	0.00	0.00	0.00	0.00	0.00	0.00	0.02	0.02	0.00	0.00	0.00	
	Depleted mantle Lu-Hf model age distributions																

Fig. 5. Pairwise comparison of U-Pb age distributions (upper right triangle) and Lu-Hf model age distributions (lower left triangle) of Quaternary sand samples. The *1-O* parameter of Andersen *et al.* (2016a) is used as a measure of difference. Sample pairs with *1-O* of zero are formally indistinguishable within error.

than 1100 Ma is, however, scarce in those deposits, but abundant both in stratigraphically higher parts of the Nama Group and in the Dwyka and Ecca groups of the Karoo Supergroup in the main Karoo Basin and the Botswana Basin (Andersen *et al.*, 2016b; Zieger *et al.*, 2019).

Samples *708*, *709*, *710* and *711* come from roadcuts through dunes between 26.7°S and 28.9°S, which is an area with Gordonia Formation dunes deposited on sedimentary rocks of the Karoo Supergroup (708 to 710) and Keis Supergroup (711). Despite the relatively long distance between the southernmost and northernmost samples, and the variation in basement, age distribution patterns are quite uniform, with major age fractions in the ranges 500 to 750 Ma and 900 to 1100 Ma, with only minor zircon in the 1100 to 1300 Ma and 1775 to 1950 Ma range (Fig. 6C). Similar distributions of Neoproterozoic and late Mesoproterozoic zircon ages have been reported from the upper part of the Nama Group (i.e. Zaris Formation and higher units, Blanco *et al.*, 2011; Hofmann *et al.*, 2015; Andersen *et al.*, 2018a), the lower part of the Karoo Supergroup in the main Karoo Basin (lower part of the Beaufort Group and below, Andersen *et al.*, 2016b) and the Dwyka and Ecca groups in the Karoo succession of southern Namibia, excluding younger zircon from tuff layers in those deposits (Zieger *et al.*, 2019).

Samples *712*, *602* and *613* are from isolated, vegetated dunes outside of the main dunefield: in the south near Kimberley (712, Fig. 2), and in the east in the Limpopo province of South Africa (Fig. 1). Sample 712 comes from a dune deposited on Archaean basement rocks of the Kaapvaal Craton, 602 from a dune on sandstone of the Clarens Formation of the Karoo Supergroup in the Thsipise Basin (Johnson *et al.*, 2006), and 613 on sandstone of the Palaeoproterozoic Wylliespoort Formation of the Soutpansberg Group (Barker *et al.*, 2006). The three samples have distribution patterns dominated by a late Neoproterozoic–Cambrian age fraction, with minor 900 to 1100 Ma zircon; samples 602 and 712 have very few grains older than this (Fig. 6D). There is also a minor but very distinct fraction of late Palaeozoic to early Mesozoic zircon in all three samples (300 to 230 Ma). This distribution pattern is very similar to that of stratigraphically higher parts of the Karoo

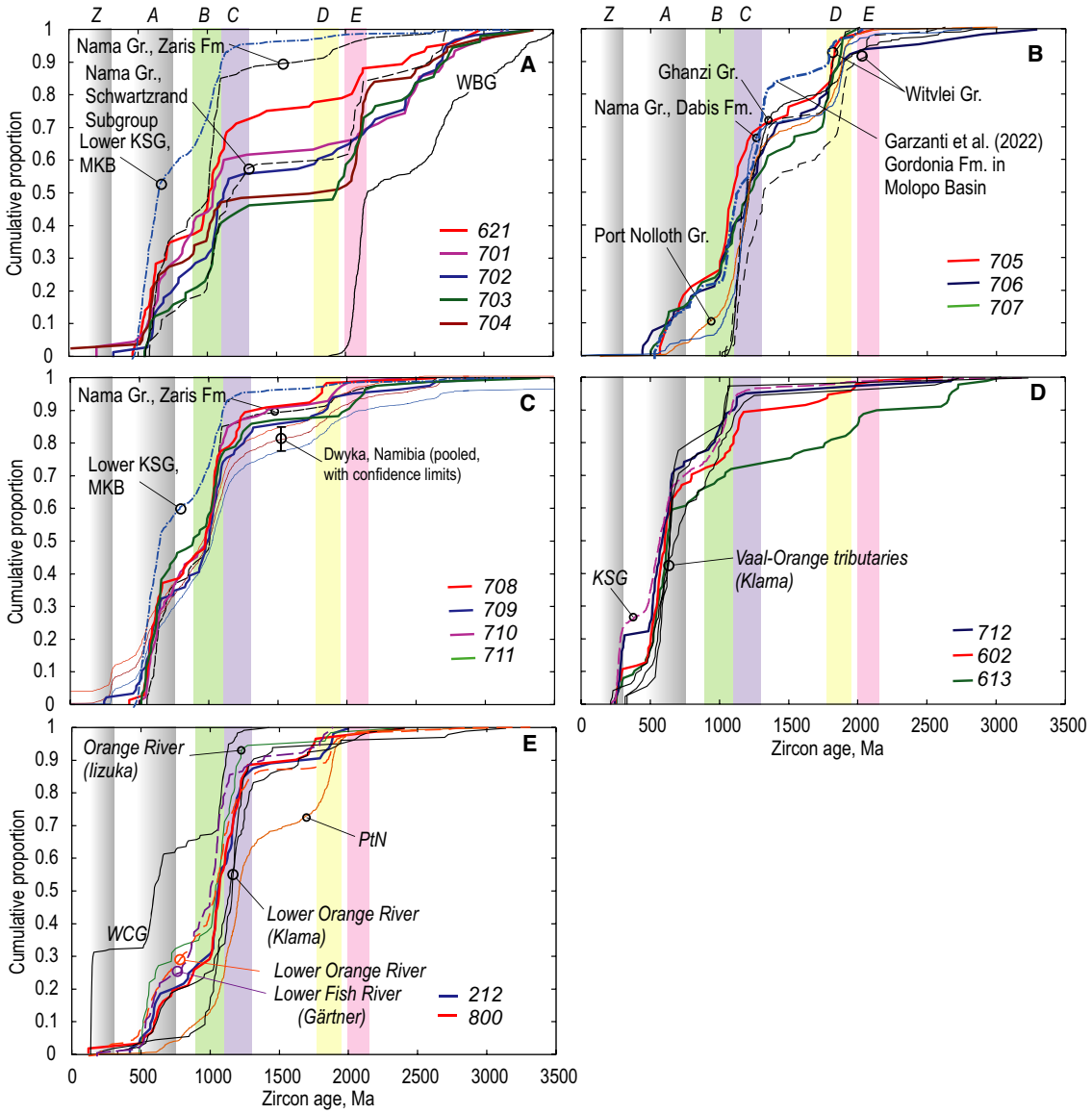

Fig. 6. Cumulative age distribution curves for detrital zircon in the samples studied, grouped according to the pairwise similarity comparison in Fig. 5. Background fields *A* to *Z* represent significant age fractions reported from previous studies of Palaeoproterozoic to Mesozoic sandstones in South Africa, see sections *Uranium–lead age distributions* and *Age fractions and 'provenance components'* in the text. (A) Samples 621 and 701 to 704. Pooled age distributions of the lower part of the Karoo Supergroup in the Main Karoo Basin (Andersen *et al.*, 2016b), Waterberg Group (Andersen *et al.*, 2019a), Zaris Formation and Schwartzrand Subgroup of the Nama Group (Blanco *et al.*, 2011; Andersen *et al.*, 2018a) are shown for comparison. (B) Age distributions for samples 705 to 707 compared to samples from the Witvlei Group, Namibia (Hofmann *et al.*, 2015), Ghanzi Group, Botswana (Hall *et al.*, 2018), Dabis Formation of the Nama Group and Port Nolloth Group of the Gariep Belt (Andersen *et al.*, 2018a). (C) Samples 708 to 711 compared to Dwyka Group in the Botswana Basin (Zieger *et al.*, 2019, 2021), lower Karoo Supergroup in the Main Karoo Basin (Andersen *et al.*, 2016b) and Zaris Formation of the Nama Group (Andersen *et al.*, 2018a). (D) Age distribution from samples 602, 613 and 712 compared to recent river sediments in southern tributaries in the Vaal–Orange river network (data from Klama, 2008) and Karoo Supergroup in the Main Karoo Basin (Andersen *et al.*, 2016b). (E) Age distributions in sand samples from the Atlantic coast compared to modern river sediment in the lower Orange and Fish rivers (Klama, 2008; Iizuka *et al.*, 2013; Gärtner *et al.*, 2021), data from Port Nolloth Group quartzite (PtN) adjacent to the sampling site of 212 (Andersen *et al.*, 2018a) and a composite of the Miocene – Holocene West Coast Group at 31°20'S (Philander & Rozendaal, 2015).

Supergroup in the Main Karoo Basin (upper Beaufort Group to Clarens Formation), which contain variable amounts of Palaeozoic zircon (Andersen *et al.*, 2016b). It is also similar to the zircon distributions for recent river sediments in southern tributaries to the Vaal–Orange river system in the area west of Kimberley (Klama, 2008). Sample 613 has additional early Palaeoproterozoic and late Archaean zircon, similar to age fractions found in the Palaeoproterozoic sandstones and conglomerates of the Waterberg and Soutpansberg groups (Andersen *et al.*, 2019a, 2020a).

The two samples of unconsolidated beach sands from the Atlantic coast (*212* and *800*), south of the Orange River mouth contain a continuous range of 900 to 1300 Ma zircon and minor late Neoproterozoic to Cambrian zircon, but very little Palaeoproterozoic zircon (Fig. 6E). Each of the samples yielded a single, Early Cretaceous zircon. The distribution of late Mesoproterozoic and Neoproterozoic zircon is similar to that of recent sediments in the lower parts of the Orange and Fish rivers (Klama, 2008; Iizuka *et al.*, 2013; Gärtner *et al.*, 2021). The scarcity of zircon in the 1750 to 1975 Ma range makes it clearly different from the local quartzites of the Port Nolloth Group of the Gariep Belt. Sample 212 was taken within one metre from the spot where sandstone sample SA14-213 of Andersen *et al.* (2018a) was collected. The sandstone has a prominent 1750 to 1975 Ma age fraction which is absent from the sand samples (Fig. 6E).

Lutetium–hafnium isotope data

In samples 621 and 701 to 704 (Fig. 7A), late Archaean and Palaeoproterozoic zircon grains range in epsilon-Hf from near zero to −10 for Archaean and to −15 for Palaeoproterozoic grains, overlapping with the field for zircon in the Waterberg Group (Andersen *et al.*, 2019a). More than half of the Mesoproterozoic to early Neoproterozoic zircon grains that were analysed for Hf isotopes give positive epsilon-Hf (zero to +10), but with a tail towards negative values, with −22 as the lowest value observed. The late Neoproterozoic–Cambrian zircon fraction shows similar minimum values, but most grains in this age fraction range from +5 to −10. Mesoproterozoic and Neoproterozoic zircon in these samples show complete overlap with corresponding age fractions in the lower part of the Karoo Supergroup in the Main Karoo Basin and the Botswana Basin (Andersen *et al.*, 2016b; Zieger *et al.*, 2019).

Regardless of age group, epsilon-Hf values in zircon from samples 705, 706 and 707 (Fig. 7B) cluster between +8 and −5, with a minor proportion of grains in each age group spreading towards negative epsilon-Hf, down to −25 in the younger age fractions. Only three grains from sample 706 show epsilon-Hf above +8. There is very close overlap between this distribution and epsilon-Hf data reported from the Port Nolloth Group in the Gariep Belt and lower part of the Nama Group (Andersen *et al.*, 2018a), and the Witvlei Group in central Namibia (Hofmann *et al.*, 2015), but less so with the Ghanzi Group of central Botswana (Hall *et al.*, 2018), in which late Mesoproterozoic zircon tends to show more positive epsilon-Hf values.

Similar to the Mesoproterozoic and Neoproterozoic zircon in samples 701 to 704, zircon in samples 708 to 711 shows ranges of epsilon-Hf from +8 to −25, with a concentration of points at low positive values (Fig. 7C). The total pattern of variation in these samples resembles that of zircon in the lower part of the Karoo Supergroup in both the Main Karoo Basin and the western part of the Botswana Basin (Andersen *et al.*, 2016b; Zieger *et al.*, 2019). A small group of points at 1100 to 1300 Ma clusters around zero; zircon with such characteristics has not been reported from the Main Karoo Basin, but constitutes a minor fraction in the Dwyka–Ecca samples from the Botswana Basin in Namibia reported by Zieger *et al.* (2019).

Despite of the considerable distance between the samples, 602, 613 and 712 show similar ranges of epsilon-Hf (Fig. 7D), with ranges from +5 to −12 in the late Palaeozoic age fraction, −16 to +5 in the Cambrian to late Neoproterozoic fraction (but with an outlier at −33), and 0 to +8 in the late Mesoproterozoic. This is within the range of zircon in the upper part of the Karoo Supergroup. Even a handful of outliers with respect to the main zircon groups in these samples fall within ranges reported for the upper part of the Karoo succession in the Main Karoo Basin by Andersen *et al.* (2016b).

Samples 212 and 800 from the Atlantic coast (Fig. 7E) have Cambrian–late Neoproterozoic and late Mesoproterozoic age fractions with epsilon-Hf from −15 to +8, with some outliers, giving complete overlap in epsilon-Hf with the distribution patterns reported from recent sediments in the lower reaches of the Orange River

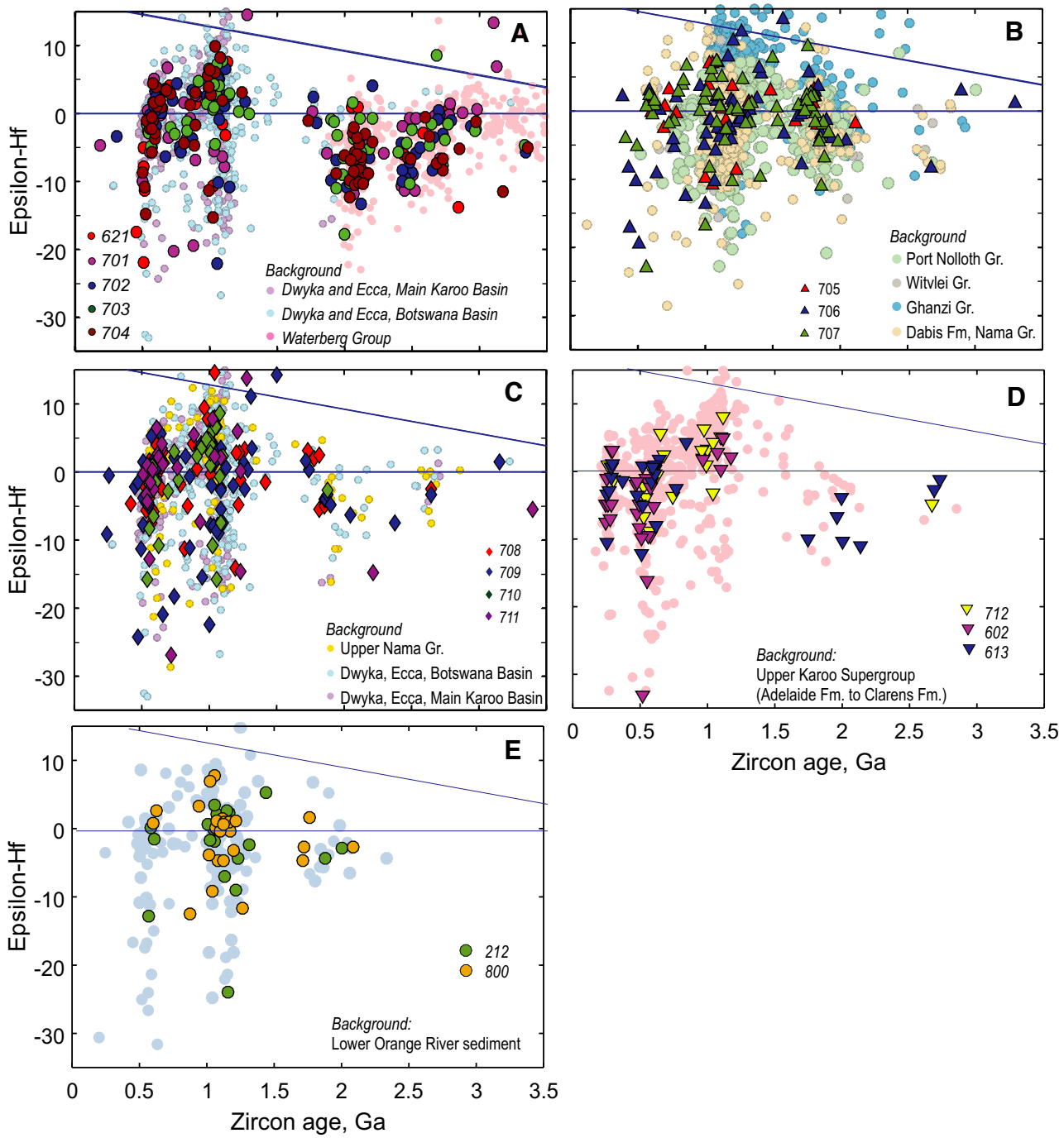

Fig. 7. Epsilon-Hf versus time diagrams of the sand samples, grouped according to the similarity criteria in Table 1, and compared to background data from older sedimentary successions in the region. Background data: Dwyka and Ecca groups in the Main Karoo Basin from Andersen *et al.* (2016b), in the Botswana Basin from Zieger *et al.* (2019, 2021), omitting younger, volcanic zircons in ash layers. Waterberg Group: Andersen *et al.* (2019a). Port Nolloth Group: Andersen *et al.* (2018a). Witvlei Group: Hofmann *et al.* (2015). Ghanzi Group: Hall *et al.* (2018). Dabis and Zaris Formation of the Nama Group: Andersen *et al.* (2018a). Upper Nama Group: Andersen *et al.* (2018a). Lower Orange River: Klama (2008), Iizuka *et al.*, (2013); Gärtner *et al.* (2021).

(Klama, 2008; Iizuka *et al.*, 2013; Gärtner *et al.*, 2021).

DISCUSSION

Age fractions and 'provenance components'

The variation of detrital zircon age distributions of the present samples illustrated in Figs 6 and 7 can be described by non-random combinations of seven distinct 'provenance components' that have previously been recorded from other sedimentary deposits in southern Africa, as shown in Table 3A and B. In the pre-Quaternary sedimentary record in the region, the *A* (500 to 750 Ma) and *B* (900 to 1100 Ma) components are characteristic in the higher part of the Nama Group (Zaris Formation and above) and the Karoo Supergroup in the Main Karoo Basin. In the Karoo Supergroup, variable amounts of the *Z* (230 to 300 Ma) component appear as clastic grains in the upper Beaufort Group and above, and in volcanic ash layers at lower stratigraphic levels (for references to occurrence of the 'age components' in Mesozoic and older deposits, see Table 3A). The lower part of the Karoo Supergroup (Dwyka and Ecca equivalents) in the Botswana Basin in Namibia also have minor contributions of the *C* (1100 to 1300 Ma) and *D* (1750 to 1975 Ma) components, which are not present at corresponding levels of the succession in the Main Karoo Basin. The *C* and *D* components are typical for the Port Nolloth Group in the Gariep Belt, and the Witvlei and Ghanzi groups in central Namibia and Botswana. In the Neoproterozoic deposits, the *A* + *B* and *C* + *D* combinations appear to be mutually exclusive (Andersen *et al.*, 2018). A combination of *E* (2000 to 2150 Ma) and *F* (2400 to 2800 Ma) components make up the detrital zircon populations of the Waterberg Group in the Waterberg and Nylstroom basins of north-eastern South Africa, but are also characteristic for sandstones of the Keis Supergroup in the Kheis Terrane (da Silva, 2011; Dreyer, 2014; van Niekerk *et al.*, 2022). The *F* component is known from the Postmasburg Group in the Griqualand West Basin, and also in Transvaal Supergroup units from the Transvaal Basin in eastern South Africa (Schröder *et al.*, 2016; Zeh *et al.*, 2020). As shown in Fig. 7, the initial epsilon-Hf values of the zircon making up each of these 'age components' in the samples of the present study are within the ranges reported in the previous studies (Andersen *et al.*, 2016b, 2018a, 2019a).

Possible protosources of components *A* to *F* have been discussed at some length by, for example, Zeh *et al.* (2016, 2020), Zieger *et al.* (2019) and Andersen *et al.* (2018, 2019a), without clear conclusions being reached. Southern Africa has been part of supercontinental assemblies (e.g. Meert, 2014) in the late Neoproterozoic – Phanerozoic (Gondwana), in the late Mesoproterozoic – early Neoproterozoic (Rodinia), and possibly in the late Palaeoproterozoic (Nuna). Zircons making up age components *A* to *F* most likely formed in mobile belts related to assembly of these supercontinents, from which they have been eroded and repeatedly recycled to their final sedimentary host (Andersen *et al.*, 2016b, 2018a, 2019a).

The *Z* component is found as detrital grains in the higher part of the Karoo Supergroup in the Main Karoo Basin (upper part of the Beaufort Group and above), with an up to 80 Ma time-lag between crystallization and final deposition. These zircon grains must have been recycled into the basin from original volcanic deposits in the Gondwanide orogen (Milani & Wit, 2008) or at the basin margin (Andersen *et al.*, 2016b). However, this component is also encountered as volcanic zircon *in situ* in ash-layers in lower parts of the Karoo Supergroup, both in the Botswana Basin (Zieger *et al.*, 2019), and in the lower part of the Beaufort Group in the Main Karoo Basin (Rubidge *et al.*, 2013).

The distribution of published U-Pb ages on igneous rocks of the Namaqua Sector of the Namaqua–Natal Belt are shown by 'barcode' diagrams in Fig. 3 (see also compiled data and references in Andersen *et al.*, 2018a). From these data, the crystalline basement in north-western South Africa would be expected to yield first-generation detrital zircon in an almost continuous age range from 900 to 1400 Ma, and between 1600 Ma and 2000 Ma. Furthermore, the Rehoboth province of Namibia would produce Mesoproterozoic detrital zircon with ages between 1400 Ma and 1600 Ma. This kind of Mesoproterozoic to Palaeoproterozoic age continuum is not seen in the detrital zircon data, where zircon between *ca* 1300 Ma and *ca* 1750 Ma is scarce or absent (Fig. 6). On the other hand, all of the age components required by the sand samples analysed in this study (Table 3B) are available in earlier sedimentary cover successions underlying or surrounding the Quaternary deposits studied here (Fig. 6), and recycling of different combinations of these will generate the observed age distributions.

Table 3. Provenance components in the dune sands.

(A) Definition of the components

	Age range (Ma)	Also present in*	References
A	500 to 750	Karoo Supergroup (KSG)	Andersen *et al.* (2016b), Zieger *et al.* (2019)
		Nama Group (Zaris Formation and higher)	Blanco *et al.* (2011), Andersen *et al.* (2018a)
B	900 to 1100	Karoo Supergroup (KSG)	Andersen *et al.* (2016b), Zieger *et al.* (2019)
		Nama Group (Zaris Formation and higher)	Blanco *et al.* (2011), Andersen *et al.* (2018a)
C	1100 to 1300	Port Nolloth Group, Gariep Belt	Basei *et al.* (2005), Andersen *et al.* (2018a) Hofmann *et al.* (2014)
		Nama Group, Dabies Formation	Andersen *et al.* (2018a)
		Dwyka and Ecca groups, Botswana Basin (minor fraction)	Zieger *et al.* (2019)
D	1750 to 1975	Port Nolloth Group, Gariep Belt	Basei *et al.* (2005), Andersen *et al.* (2018a), Hofmann *et al.* (2014)
		Dabies Formation, Nama Group	Andersen *et al.* (2018a)
		Witvlei Group, central Namibia	Hofmann *et al.* (2015)
		Ghanzi Group, Botswana	Hall *et al.* (2018)
		Dwyka and Ecca groups, Botswana Basin (minor fraction)	Zieger *et al.* (2019)
E	2000 to 2150	Waterberg Group	Andersen *et al.* (2019a)
		Keis Supergroup	Da Silva (2011), Dreyer (2014), Van Niekerk *et al.* (2022)
F	2400 to 2800	Griqualand West Basin	Moore *et al.* (2012b)
Z	230 to 300	Detrital grains in upper part of KSG, MKB	Andersen *et al.* (2016b)
		Tuff-layers in Ecca and Dyka groups, Botswana Basin	Bangert *et al.* (1999)
		Tuff-layers in KSG, MKB	Rubidge *et al.* (2013)

(B) Combinations observed in the in the dune sands

Samples	Major age fractions	Minor age fractions
621, 701 to 704	A + B + E + F	C + D (702 only)
705 to 707	C + D	A + B
708 to 711	A + B	E (711), C + D (708, 710), D (709)
712	A + B + Z	
212, 800	A + B	C + D

* As major age fractions, unless otherwise stated.

Late Cretaceous–Cenozoic sediment transport in southern Africa: Rivers, wind and current

Quaternary recycling, transport and deposition processes must be seen in the context of the geomorphological evolution of southern Africa during the Cenozoic (e.g. Partridge & Maud, 1987). The drainage pattern of southern Africa has evolved in response to tectonic events, erosion and variations in rainfall over the region. At present, interior South Africa is drained to the Atlantic coast by the perennial Vaal–Orange river system with a large network of tributaries (Fig. 8A). The lower Orange River is connected to the southern part of the Kalahari Basin by the dry courses of the Auob–Nossob–Molopo–Kuruman river system (Fig. 9).

Whereas the lower courses of the Orange River appear to have been more or less constant since the Late Cretaceous, the connection to the upper part of the present-day Orange–Vaal river network may have evolved with time (Fig. 8B). In the Late Cretaceous (*ca* 100 Ma), interior South Africa was drained to the Atlantic coast by two major, west-flowing rivers: the Kalahari (or

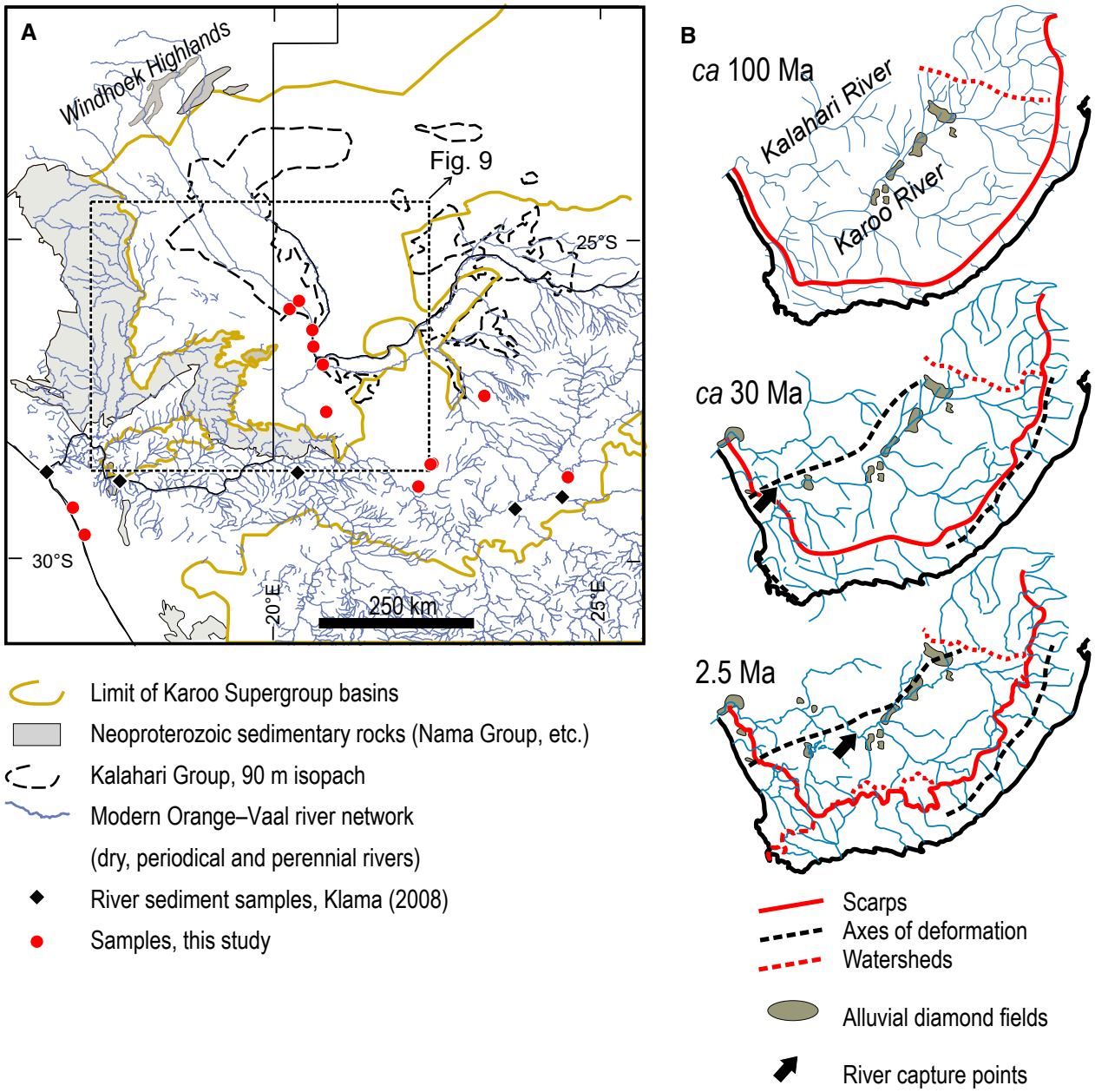

Fig. 8. (A) The complete, modern drainage network of the area shown in Fig. 2. Outline of Karoo Supergroup and Nama Group as in Fig. 2, the 90 m isopach of the Kalahari Group is from Haddon (2005). The river network is from shapefiles downloaded from the Department of Water Affairs, South Africa, 2016. Samples of the present study are shown as in Fig. 2, with samples of modern river sediments analysed by Klama (2008). (B) Evolution of drainage network in South Africa since the Cretaceous according to de Wit (1999), with position of the Great Escarpment, major watersheds and deformation axes of major Cretaceous–Cenozoic uplift events in the region (Partridge & Maud, 1987). Alluvial diamond fields from Lynn (1998). According to this model, the Cretaceous Karoo river was captured by the Orange River in events indicated by arrows. The existence of a Karoo River is not universally accepted, for an alternative scenario, in which the area is drained by the Orange or Kalahari River throughout the period, see Moore & Moore (2004).

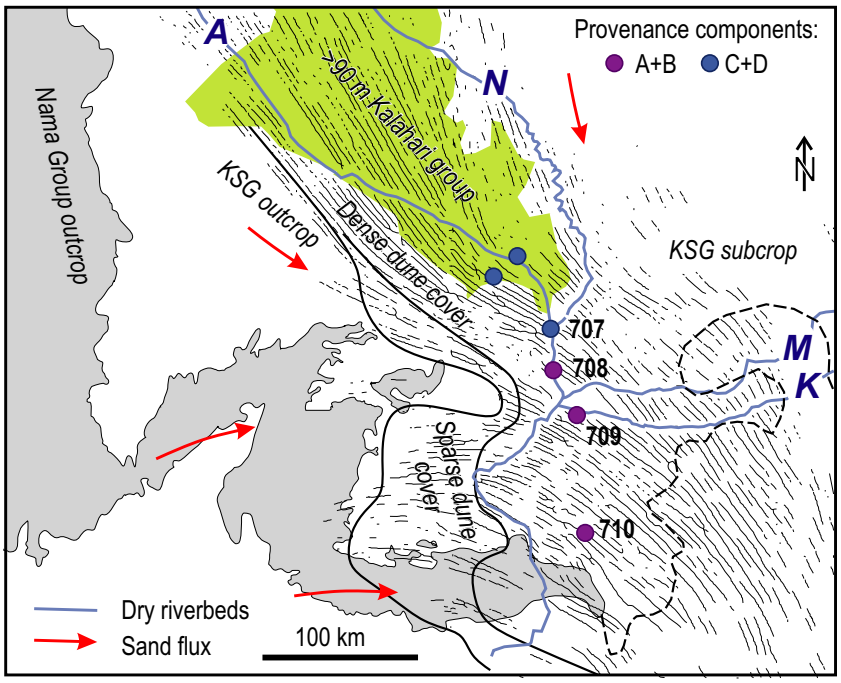

Fig. 9. Detail from Fig. 8, showing the positions of samples 705 to 710 (cf. Fig. 2) with respect to the dune pattern according to Lancaster (1981), dry river beds of the Auob (A), Nossob (N), Molopo (M) and Kuruman (K) rivers, and resultant sand-drift vectors from Heine (1982). The grey field is the outcrop of the Nama Group in southern Namibia (from Vickers-Rich *et al.*, 2016). Sedimentary rocks of the Karoo Supergroup crop out east and north of the Nama Group; the southern limit of Karoo Supergroup in subcrop is shown by a broken line (from Catuneanu *et al.*, 2005). The fields of outcrop, sparse dune cover and dense dune cover are derived from maps of Lancaster (1981), Heine (1982), Thomas & Shaw (1991) and Google Earth© images. The field of >90 m thickness of Kalahari Group (green) is based on the isopach map of the Kalahari Group in Haddon (2005).

palaeo-Orange) River in the north, and a southern Karoo River (de Wit, 1999; Kounev *et al.*, 2008), or by a single river system similar to the present-day Vaal–Orange network (Moore & Moore, 2004). If a Late Cretaceous Karoo River existed, its upper courses must have been captured by the lower Orange River in a series of events in Miocene to Pliocene time (de Wit, 1999), as indicated by arrows in Fig. 8B. In either of these scenarios, northward and westward river transport of material eroded off the uplifted Main Karoo Basin in the south has been more or less continuously possible from the Late Cretaceous to the present. Independent evidence of northward recycling of material from the Main Karoo Basin is given by the occurrence of alluvial diamond deposits in interior South Africa (Fig. 8B). Diamonds in these deposits were partly derived from post-Cretaceous kimberlites within the Kaapvaal Craton, and partly remobilized by erosion of sedimentary rocks of the Karoo Supergroup, mainly glaciogenic sediments of the Dwyka Group containing diamonds from older kimberlites. Diamondiferous material was moved across the former Cargonian Highlands and eventually into the lower reaches of the Orange River in Cretaceous and Cenozoic time (Lynn, 1998; Moore & Moore, 2004).

From the Late Palaeogene (*ca* 30 Ma), the Kalahari Basin was connected to a northern river system comprising the Okavango, Upper Zambezi, Kafue, Cuando and palaeo-Chambeshi rivers, with headwaters in southern Central Africa north of 10°S, allowing detritus from distal sources to be fed into the basin (Vainer *et al.*, 2018). This drainage system may have been connected to the Kalahari/palaeo-Orange river by the Molopo (Bootsman, 1998) or the hypothetical Trans-Tswana river (McCarthy, 1983). This connection was severed by uplift across the southern Kalahari, and successive river capture events in the Zambezi and Congo systems in the Pliocene and early Pleistocene eventually diverted the northern rivers from the Kalahari

Basin (Key *et al.*, 2015), so that the only major river feeding the basin from the north at the present time is the Okavango. Cut off from its major water supply, the Kalahari Basin gradually dried out during Pleistocene – Holocene time, but with reactivation of rivers in periods of high rainfall (Moore *et al.*, 2012a).

In the south-western Kalahari, the Auob–Nossob river system has been active in humid periods, in Pleistocene and Holocene time, with a major period of activity starting around 1.0 Ma, (which is also a period of rapid sedimentation in other watercourses in the southern Kalahari, Matmon *et al.*, 2015), and lasting until 235 to 500 ka (Miller, 2014). At present, the rivers carry water only infrequently, during periods with high rainfall in the source areas (Thomas & Shaw, 1991). The headwaters of the Pleistocene–Holocene drainage basins of the Auob and Nossob rivers are in the Windhoek Highlands in central Namibia (Strobach, 2008), at the front of the Neoproterozoic Damara orogenic belt (Corner & Durrheim, 2018). The Auob and Nossob river valleys coincide with areas of thick Kalahari Group valley-fill (Figs 7 to 9). The Auob–Nossob drainage basin was connected to the Kalahari or palaeo-Orange river already in the Cretaceous (Bootsman, 1998; de Wit, 1999), indicating that southward transport of material from as far north as the Damara front into the lower Orange River has been possible both in Cretaceous time and during later, humid, periods.

Aeolian sediment transport has been dominant in the Kalahari Basin in arid periods from the Pliocene to the present. Stable, linear dunes develop parallel to the dominant wind direction, or to the resultant of divergent wind directions (e.g. Pye & Tsoar, 2009). Directions of dune axes in the Kalahari have been interpreted in terms of an atmospheric circulation pattern over southern Africa compatible with arid conditions (Lancaster, 1981). In the southern part of the Kalahari sand field, dune axes, and thereby resultant sand drift directions, vary from south-east in the north to east/south-east and east in the south (Fig. 9). Linear dune formation may have started as early as *ca* 4 Ma, and was certainly well-advanced when dunes were cut by the Auob River at *ca* 1.0 Ma (Miller, 2014). Subsequent periods of dune development in late Pleistocene and Holocene time are recorded by cosmogenic nuclide and luminescence dating (Matmon *et al.*, 2015; Thomas & Burrough, 2016; Stone, 2021). At present, dunes are mainly dormant or partially active, with limited remobilization of sand along dune crests (Telfer & Thomas, 2007).

Material transported by the Orange River may be a major component in the West Coast Group and overlying beach and dune sand south of the river mouth, but wind and wave-driven longshore drift may have added material from unconsolidated deposits further south along the coast (Garzanti *et al.*, 2012). Coast-parallel drift from the south is enhanced by prevailing winds in the summer season, whereas winds from the south-west, mainly in the winter season, can move sand towards the interior (Fig. 10).

Detrital zircon, provenance components and sedimentary recycling

The common denominator: recycling of Karoo Supergroup and Nama Group

The combination of the $A + B \pm Z$ (i.e. <1100 Ma) provenance components is characteristic for the Karoo Supergroup in both the Main Karoo Basin and the Botswana Basin (see references in Table 3A). The simultaneous presence of *A, B* and *Z* components in younger deposits, including the Cretaceous Boane sandstone of southern Mozambique, Cretaceous to Palaeogene sediments in the Lundi (Zimbabwe) and Oliphants (Mozambique) river valleys (Andersen *et al.*, 2020a), Miocene to recent sands in KwaZulu–Natal (Andersen *et al.*, 2016a) and Miocene to Holocene sands of the West Coast Group (Philander & Rozendaal, 2015) indicates that recycling of the Karoo Supergroup has been an important process in the region since breakup of the Gondwana Supercontinent.

Major amounts of the *A* and *B* components are present in sample 602 deposited on rocks of the Karoo Supergroup, but also in samples 613, 621, 701 to 704, 711 and 712 from areas with no *in situ* Karoo Supergroup cover (Figs 1 and 2). Recycled material from the lower part of the Karoo Supergroup (Dwyka and Ecca groups) of the Main Karoo Basin may have been transported into this area after Gondwana breakup and crustal uplift to the south, as envisaged by Moore & Moore (2004). Furthermore, the wide, southern tributary networks of the modern Orange and Vaal rivers overlap with outcrop of Dwyka and Ecca groups of the Main Karoo Basin (Fig. 8A). Modern river sediments in the middle part of the Orange River show a distinct $A + B$ character (Klama, 2008, see Fig. 4D), suggesting that more recent input of such material into the former Cargonian Highlands has also been

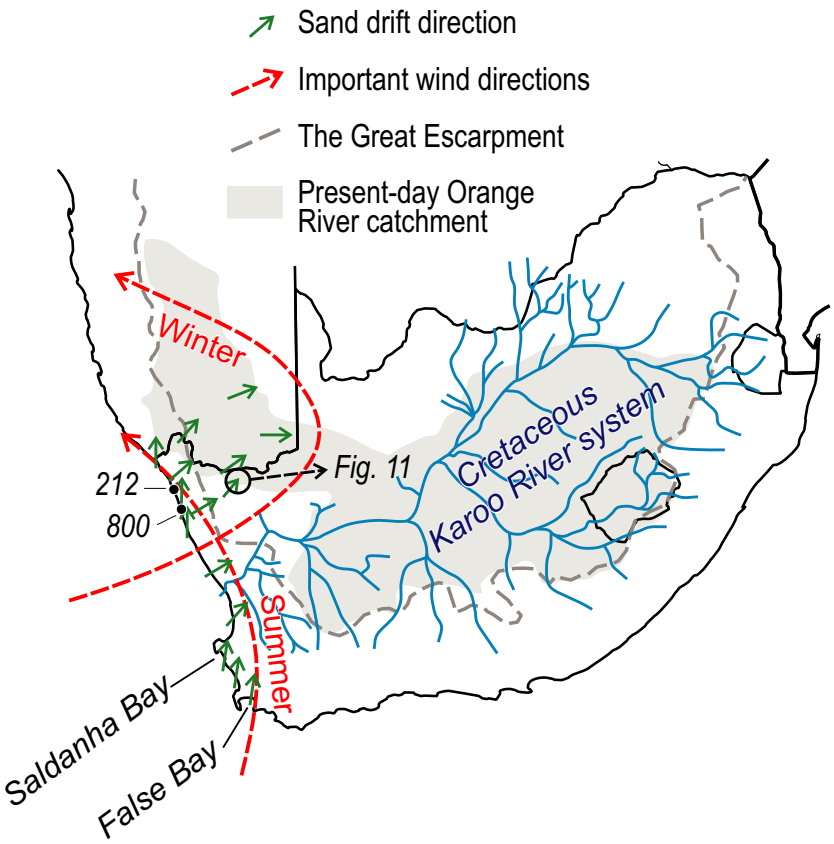

Fig. 10. Possible wind and wave-driven sedimentary recycling along the Atlantic coast. Wind directions are from Kruger *et al.* (2010), the Cretaceous Karoo River system from de Wit (1999) and sand drift directions from Heine (1982), Chase & Thomas (2006), Roberts *et al.* (2013) and Philander & Rozendaal (2015). The three southernmost sand drift arrows represent inland wind-driven transport in the False Bay – Saldanha Bay area, from Roberts *et al.* (2013).

possible. The presence of *A* + *B* components in these dunes thus indicates that detritus transported by rivers from the south has been followed by local aeolian remobilization.

The presence of *A* + *B* components in samples 708 to 710 from north of the Orange River is less likely to be due to transport from the south. However, Dwyka and Ecca Group deposits occur in subcrop in the area (Figs 2 and 7). Immediately west of the dunefield are areas with sparse dune cover and exposures of lower Karoo Supergroup of the Botswana Basin and of the upper part of the Nama Group, both of which carry an *A* + *B* signature (Fig. 8). Sand drift directions in the area are towards south-east and east, suggesting that material with the required detrital zircon signature from the basin margin by wind is a feasible mechanism.

The minor amount of components *A* + *B* in the samples from the Atlantic coast (212 and 800) match the distribution of these components in recent sediments from the lower reaches of the Orange River (Klama, 2008; Iizuka *et al.*, 2013; Gärtner *et al.*, 2021; see Fig. 6E). The Orange River itself may have transported already remobilized lower Karoo detritus from distal sources in the south or east, or it may have been fed by recycled upper Nama Group material from the catchment of the Fish River (Figs 8A and 9). However, the Cenozoic West Coast Group at 31°20′S contains, in addition to zircon from local, Cretaceous intrusions, *A* and *B* components (Philander & Rozendaal, 2015), the source of which is undoubtedly in the Main Karoo Basin (Fig. 6E). After Gondwana breakup, the Karoo River and/or other westward flowing rivers transported massive amounts of detritus from the Karoo Supergroup towards the western seaboard (Fig. 10). Subsequent transport by wind-driven and wave-driven longshore drift in the summer season will move such material northward, which may have contributed to the

A + *B* content in samples 212 and 800. Aeolian transport of material from the West Coast Group towards the inland by winds from the south-west in winter is suggested by dune morphology at several localities along the west coast and inland in north-western South Africa and southern Namibia (Fig. 10).

Landward transport of aeolian sand from coastal deposits has been documented from False Bay to Saldanha Bay in south-westernmost South Africa (Fig. 10), where it is driven by dominant winds in the summer season (Roberts *et al.*, 2013), and in the coastal sandfields of Namibia, where it extends several tens of kilometres inland (Lancaster, 1982; Lancaster & Ollier, 1983; Garzanti *et al.*, 2015). Furthermore, Fig. 11 shows an example of linear dunes with deflection structures around a group of inselbergs *ca* 150 km inland from the coast in north-western South Africa (at the location marked in Fig. 10), indicating that north-eastward aeolian sand drift extends well into the interior, eventually to reach the lower Orange River valley. When combined with river transport back towards the sea, this amounts to a possible recycling cell in which detritus containing *A* + *B* zircon is exchanged between coastal deposits and the lower Orange River.

Recycling of pre-Karoo sedimentary rocks

Samples 621 and 701 to 704 come from dunes deposited on Palaeoproterozoic–Mesoproterozoic basement. The characteristic *E* and *F* components (i.e. ages >2 Ga) in these samples must be of a local origin, related to remobilization of sedimentary successions in the Kheis Terrane and possibly (for the *F*-component in 621), the Transvaal Supergroup in the Griqualand West Basin.

Samples 705, 706 and 707 have major amounts of the *C* and *D* components (1.10 to 1.30 and 1.75 to 1.98 Ga), otherwise only found in Lower Neoproterozoic deposits in the region. Transport from the Gariep Belt in north-western South Africa and south-western Namibia would be against both prevalent wind directions and river gradients, and can therefore be ruled out as a major process. Lower Neoproterozoic sedimentary rocks of the Witvlei and Ghanzi groups crop out along the Damara front in Namibia and

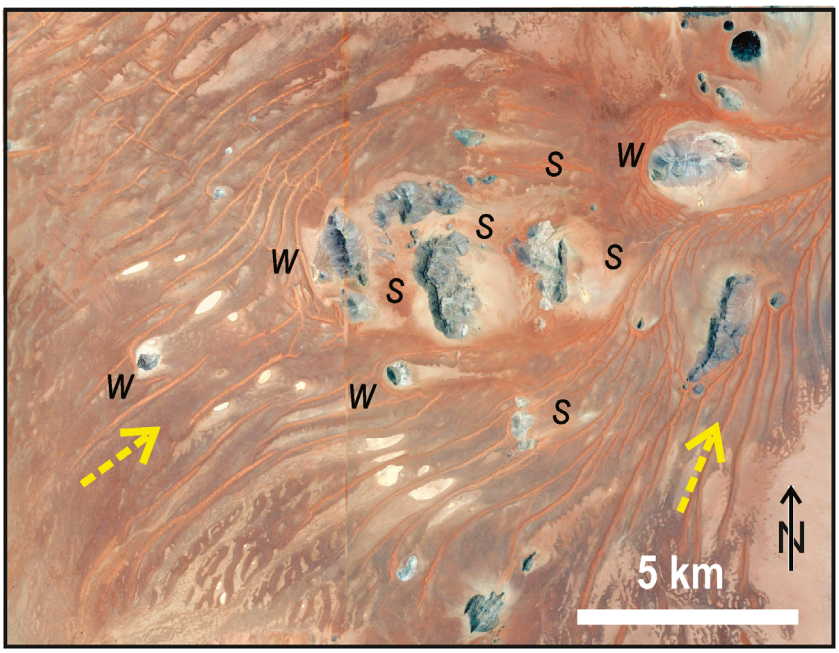

Fig. 11. Google Earth© image showing linear dunes in the north-western part of the Koa Valley Dune field (Botha, 2021), deflected around topographic obstacles formed by a group of inselbergs at 29°10′S, 18°26′E, *ca* 150 km inland from the Atlantic coast and 25 km south of the Orange River, at the point indicated in Fig. 9. The linear dune directions at 25° to 55°, shown by arrows, indicate sand drift from SSW and south-west. Horseshoe-shaped deflection structures have formed around the inselbergs, with well-developed echo or windward dunes (Mabbutt, 1977; Pye & Tsoar, 2009) upwind and less well-developed shadow or lee dunes downwind, marked by *W* and *S*, respectively.

Botswana (Fig. 2; Modie, 2000; Prave *et al.*, 2011). These have detrital zircon age distributions dominated by the *C* and *D* components (Fig. 6B); rocks of the Witvlei Group are more likely precursors than the Ghanzi Group, because of the consistently higher epsilon-Hf values of detrital zircon in the latter (Fig, 7B; Hall *et al.*, 2018; Hofmann *et al.*, 2015). Southward fluvial transport from the northern part of the Auob and Nossob drainages would have been possible during periods when these rivers were active, followed by local aeolian remobilization of Kalahari Group sediments within the river basin.

There is a significant change in detrital zircon age patterns over the *ca* 30 km distance between samples 707 and 708, with diminishing contents of the $C + D$ components southward (Figs 6B, 6C and 9). This is correlated with a change in dune orientation, from 130° in the north to 110°, corresponding to changes in wind-borne sand flow (Fig. 9). The increase of *A* and *B* components southward to sample 708 suggests a rapidly increasing effect in this area of wind-transported material from Karoo Supergroup and Nama Group exposures west of the basin. Downstream transport of the *C* and *D* components into the lower Orange River from sources in the north was, however, possible during periods of active flow in the Auob and Nossob rivers.

IMPLICATIONS

The sands analysed in the present study were deposited over a short (in geological terms) time interval in the late Pleistocene – Holocene, and over a limited part of a much larger basin. Nevertheless, the entire spectrum of detrital zircon age fractions observed in Palaeoproterozoic to Phanerozoic sedimentary precursors in the region occur in the sands, in combinations and proportions that vary over the area. This rather complex detrital zircon signature is an effect of mixing and deposition of recycled material derived from pre-existing cover successions with different ages and provenance characteristics, followed by remobilization of detritus by water and wind within the basin itself.

Because: (i) the detrital zircon distributions of pre-Cenozoic cover successions in the region are known from earlier studies; (ii) the transport processes and basin filling history are well-constrained; and (iii) the sediments are unaffected by post-depositional tectonism, deformation and metamorphism, it is possible to work out a reasonable model for sources and routing of sediment. This is a situation one should not expect to meet when studying older, less well-exposed sedimentary units that may also have been deformed, metamorphosed and fragmented by tectonic displacement. If the sediments analysed here had been encountered in drillcores through an unexposed succession, or as fragments in a foldbelt, they could invite very misleading provenance and cross-basin correlation models. The results presented here can serve as a further illustration that protosource information from detrital zircon needs to be supported by independent information relating to the existence and characteristics of older sedimentary cover sequences and the past and present transport regime to give a meaningful contribution to basin evolution studies. Detrital zircon ages and Hf isotope compositions should only be invoked as provenance indicators when there is independent evidence that the sediments studied are derived directly from crystalline protosource rocks.

The possible existence of an active recycling system in the coastal region and the lower ranges of the Orange River illustrate a further complication: River transport from upstream and wind transport from the coast will bring material that is indistinguishable in terms of detrital zircon signature into the western part of the Orange River catchment. Detrital zircon data cannot be used to distinguish between such scenarios.

CONCLUSIONS

The control on the detrital zircon signature of Quaternary dune sands in the Northern Cape Province of South Africa is an interplay of the local basement geology at the site of the dune, the distribution of older cover rocks around the basin, the evolution of the river network within and around the basin, and the filling history of the basin from the Cretaceous to the Pleistocene. The Karoo Supergroup is the youngest of the widely distributed pre-existing cover successions in southern Africa, it is the most widely exposed, and also the least consolidated of the sedimentary precursors. Where Karoo strata have been available, they have provided a fertile source of recyclable detritus, either through river transport, or by aeolian remobilization of regoliths or already remobilized material. Because nearly all of the limiting factors (basement geology and sedimentary precursors, drainage evolution and aeolian transport, detrital zircon

distributions of sedimentary precursors) are well-constrained, detrital zircon data on the sediments can contribute to a reasonable basin filling history, despite the lack of direct protosource-to-final-sink transport, which is the positive finding of this study.

On the negative side, this study shows that sedimentary strata deposited in a minor part of a larger basin, during a relatively short period of time can show very considerable variation in terms of detrital zircon distribution patterns. If sedimentary rocks with a similar variation in detrital zircon distribution patterns were encountered out of their proper stratigraphic context, or without the supporting information invoked here, unsupported detrital zircon data may invite problematic interpretations.

The bottom line of this study is that the detrital zircon distribution pattern of a suite of sediments is likely to reflect sedimentological controls, basin dynamics and recycling history as much as provenance. The results should serve as a warning against the uncritical use of protosource information contained in detrital zircon as an indicator of 'source-to-sink' transport of detritus.

ACKNOWLEDGEMENTS

The LA-MC-ICPMS laboratory at UJ was funded from NRF-NEP grant #93208. Henriette Ueckermann (UJ) and Magnus Kristoffersen (UiO) are acknowledged for their help with the U-Pb and Hf isotopic analyses, and Siri Simonsen for CL imaging. MAE acknowledges funding from an NRF IPRR grant 119297. The support of the DSI-NRF Centre of Excellence (CoE) for Integrated Mineral and Energy Resource Analysis (DSI-NRF CIMERA) towards this research is hereby acknowledged. Opinions expressed and conclusions arrived at, are those of the author(s) and are not necessarily to be attributed to the CoE. TA acknowledges funding from the Department of Geoscience, University of Oslo through the Småforsk programme 2019 and 2020 (no grant numbers). Helpful comments from Eduardo Garzanti and an anonymous reviewer are gratefully acknowledged.

CONFLICTS OF INTEREST

The authors know of no conflict of interest in connection with this work.

DATA AVAILABILITY STATEMENT

Data to support this study are available in the supplementary material.

REFERENCES

Andersen, T. (2002) Correction of common lead in U-Pb analyses that do not report ^{204}Pb. *Chem. Geol.*, **192**, 59–79.

Andersen, T., **Botha, G.A.** and **Elburg, M.A.** (2020a) A late Mesozoic – early Cenozoic sedimentary recycling system on the Gondwana rifted margin of SE Africa. *S. Afr. J. Geol.*, **123**, 343–356.

Andersen, T. and **Elburg, M.A.** (2022) Open-system behaviour of detrital zircon during weathering: an example from the Palaeoproterozoic Pretoria Group, South Africa. *Geol. Mag.*, **159**, 561–576.

Andersen, T., **Elburg, M.** and **Cawthorn-Blazeby, A.** (2016a) U-Pb and Lu-Hf zircon data in young sediments reflect sedimentary recycling in eastern South Africa. *J. Geol. Soc. London*, **173**, 337–351.

Andersen, T., **Elburg, M.A.** and **Lehmann, J.** (2020b) Enigmatic provenance signature of sandstone from the Okwa Group, Botswana. *S. Afr. J. Geol.*, **123**, 331–342.

Andersen, T., **Elburg, M.A.**, **van Niekerk, H.S.** and **Ueckermann, H.** (2018a) Successive sedimentary recycling regimes in southwestern Gondwana: evidence from detrital zircons in Neoproterozoic to Cambrian sedimentary rocks in southern Africa. *Earth Sci. Rev.*, **181**, 43–60.

Andersen, T., **Elburg, M.A.** and **Magwaza, B.** (2019b) Sources of bias in detrital zircon geochronology: discordance, concealed lead loss and common lead correction. *Earth Sci. Rev.*, **197**, 102899.

Andersen, T., **Elburg, M.A.** and **Van Niekerk, H.S.** (2019a) Detrital zircon in sandstones from the Palaeoproterozoic Waterberg and Nylstroom basins, South Africa: provenance and recycling. *S. Afr. J. Geol.*, **122**, 79–96.

Andersen, T., **Kristoffersen, M.** and **Elburg, M.** (2016b) How far can we trust provenance and crustal evolution information from detrital zircon? A South African case study. *Gondwana Res.*, **34**, 129–148.

Andersen, T., **Kristoffersen, M.** and **Elburg, M.A.** (2018b) Visualizing, interpreting and comparing detrital zircon age and Hf isotope data in basin analysis – a graphical approach. *Basin Res.*, **30**, 132–147.

Andersen, T., **Sayeed, A.**, **Gabrielsen, R.H.** and **Olaussen, S.** (2011) Provenance characteristics of the Brumunddal sandstone in the Oslo Rift derived from U-Pb, Lu-Hf and trace element analyses of detrital zircons by laser ablation ICMPS. *Nor. J. Geol.*, **91**, 1–19.

Bailie, R., **Armstrong, R.** and **Reid, D.** (2007) The Bushmanland Group supracrustal succession, Aggeneys, Bushmanland, South Africa: provenance, age of deposition and metamorphism. *S. Afr. J. Geol.*, **110**, 59–86.

Bangert, B., **Stollhofen, H.**, **Lorenz, V.** and **Armstrong, R.** (1999) The geochronology and significance of ash-fall tuffs in the glaciogenic Carboniferous-Permian Dwyka Group of Namibia and South Africa. *J. Afr. Earth Sci.*, **29**, 33–49.

Barker, O.B., **Brandl, G.**, **Callaghan, C.C.**, **Eriksson, P.G.** and **van der Neut, M.** (2006) The Soutpansberg and Waterberg Groups and the Blouberg formation. In: *The Geology of*

South Africa (Eds Johnson, M.R., Anhaeusser, C.R. and Thomas, R.J.), *Geol. Soc. S. Afr.*, 301–318.

Basei, M.A.S., **Frimmel, H.E.**, **Nutman, A.P.**, **Preciozzi, F.** and **Jacob, J.** (2005) A connection between the Neoproterozoic Dom Feliciano (Brazil/Uruguay) and Gariep (Namibia/South Africa) orogenic belts – evidence from a reconnaissance provenance study. *Precambrian Res.*, **139**, 195–221.

Belousova, E.A., **Kostitsyn, Y.A.**, **Griffin, W.L.**, **Begg, G.C.**, **O'Reilly, S.Y.** and **Pearson, N.J.** (2010) The growth of the continental crust: constraints from zircon Hf-isotope data. *Lithos*, **119**, 457–466.

Blanco, G., **Germs, G.J.B.**, **Rajesh, H.M.**, **Chemale, F.**, **Dussin, I.A.** and **Justino, D.** (2011) Provenance and paleogeography of the Nama Group (Ediacaran to early Palaeozoic, Namibia): petrography, geochemistry and U-Pb detrital zircon geochronology. *Precambrian Res.*, **187**, 15–32.

Blatt, H. (1967) Provenance determinations and recycling of sediments. *J. Sed. Petrol.*, **37**, 1031–1044.

Bootsman, C.S. (1998) The evolution of the Molopo Drainage. PhD thesis, University of the Witwatersrand, Johannesburg, South Africa, 262 pp. Available at: http://hdl.handle.net/10539/20876

Botha, G.A. (2021) Cenozoic stratigraphy of South Africa: current challenges and future possibilities. *S. Afr. J. Geol.*, **124**, 817–842.

Botha, G.A. and **de Wit, M.C.J.** (1996) Post-Gondwanan continental sedimentation, Limpopo region, southeastern Africa. *J. Afr. Earth Sci.*, **23**, 163–187.

Bouvier, A., **Vervoort, J.D.** and **Patchett, P.J.** (2008) The Lu-Hf and Sm-Nd isotopic composition of CHUR: constraints from unequilibrated chondrites and implications for the bulk composition of terrestrial planets. *Earth Planet. Sci. Lett.*, **273**, 48–57.

Browning, C. and **Roberts, D.L.** (2015) Lithostratigraphy of the Witzand Formation (Sandveld Group), South Africa. *S. Afr. J. Geol.*, **118**, 317–322.

Catuneanu, O., **Wopfner, H.**, **Eriksson, P.G.**, **Cairncross, B.**, **Rubidge, B.S.**, **Smith, R.M.H.** and **Hancox, P.J.** (2005) The Karoo basins of south-central Africa. *J. Afr. Earth Sci.*, **43**, 211–253.

Chase, B.M. and **Thomas, D.S.G.** (2006) Late Quaternary dune accumulation along the western margin of South Africa: distinguishing forcing mechanisms through the analysis of migratory dune forms. *Earth Planet. Sci. Lett.*, **251**, 318–333.

Condie, K.C., **Bickford, M.E.**, **Aster, R.C.**, **Belousova, E.A.** and **Scholl, D.W.** (2011) Episodic zircon ages, Hf isotopic composition, and the preservation rate of continental crust. *Geol. Soc. Am. Bull.*, **123**, 951–957.

Cornell, D.H., **Thomas, R.J.**, **Moen, H.F.G.**, **Reid, D.L.**, **Moore, J.M.** and **Gibson, R.L.** (2006) The Namaqua-Natal Belt. In: *The Geology of South Africa* (Eds Johnson, M.R., Anhaeusser, C.R. and Thomas, R.J.), *Geol. Soc. S. Afr.*, 325–379.

Corner, B. and **Durrheim, R.J.** (2018) An integrated geophysical and geological interpretation of the Southern African lithosphere. In: *Geology of Southwest Gondwana* (Eds Siegesmund, S., Basei, M.A.S., Oyhantcabal, P. and Oriolo, S.), *Reg. Geol. Rev.*, 19–61.

Cox, R., **Lowe, D.R.** and **Culles, R.L.** (1995) The influence of sediment recycling and basement composition on evolution of mudrock chemistry in the southwestern United States. *Geochim. Cosmochim. Acta*, **59**, 2919–2940.

De Beer, C.H. (2010) The geology of the Garies area. Explanation of 1:250 000-scale map sheet 3017 Garies. *Coun. Geosci. S. Afr.*, 100 pp.

Dickinson, W.R., **Lawton, T.F.** and **Gehrels, G.E.** (2009) Recycling detrital zircons: a case study from the cretaceous Bisbee group of southern Arizona. *Geology*, **37**, 503–506.

Dreyer, D. (2014) Provenance an age of Palaeoproterozoic red beds of the Elim Group (Griqualand West, South Africa) as determined from detrital zircon age populations. MSc thesis, University of Johannesburg, South Africa, 206 pp.

Elburg, M.A., **Andersen, T.**, **Bons, P.D.**, **Simonsen, S.L.** and **Weisheit, A.** (2013) New constraints on Phanerozoic magmatic and hydrothermal events in the Mt Painter Province, South Australia. *Gondwana Res.*, **24**, 700–712.

Eriksson, R.G., **Altermann, W.** and **Hartzer, F.J.** (2006) The Transvaal supergroup and its precursors. In: *The Geology of South Africa* (Eds Johnson, M.R., Anhaeusser, C.R. and Thomas, R.J.), *Geol. Soc. S. Afr.*, 237–260.

Fedo, C.M., **Sircombe, K.N.** and **Rainbird, R.H.** (2003) Detrital zircon analysis of the sedimentary record. *Rev. Mineral. Geochem.*, **53**, 277–303.

Foster, D.A., **Goscombe, B.D.**, **Newstead, B.**, **Mapani, B.**, **Mueller, P.A.**, **Gregory, L.C.** and **Muvangua, E.** (2015) U-Pb age and Lu–Hf isotopic data of detrital zircons from the Neoproterozoic Damara sequence: implications for Congo and Kalahari before Gondwana. *Gondwana Res.*, **28**, 179–190.

Franceschini, G., **Compton, J.S.** and **Wigley, R.A.** (2003) Sand transport along the Western Cape coast: gone with the wind*? S. Afr. J. Sci.*, **99**, 317–318.

Gärtner, A., **Hofmann, M.**, **Zieger, J.**, **Sagwe, A.**, **Krause, R.**, **Stutzriemer, M.**, **Gesang, S.**, **Gerdes, A.**, **Marko, L.**, **Lana, X.** and **Linnemann, U.** (2021) Implications for sedimentary transport processes in southwestern Africa: a combined zircon morphology and age study including extensive geochronology databases. *Int. J. Earth Sci.*, **111**, 767–788.

Garzanti, E., **Andò, S.**, **Vezzoli, G.**, **Lustrino, M.**, **Boi, M.** and **Vermesch, P.** (2012) Petrology of the Namib Sand Sea: long-distance transport and compositional variability in the wind-displaced Orange Delta. *Earth Sci. Rev.*, **112**, 173–189.

Garzanti, E., **Pastore, G.**, **Stone, A.**, **Vainer, S.**, **Vermeesch, P.** and **Resentini, A.** (2022) Provenance of Kalahari Sand: Paleoweathering and recycling in a linked fluvial-aeolian system. *Earth Sci. Rev.*, **224**, 103867.

Garzanti, E., **Resentini, A.**, **Andò, S.**, **Vezzoli, G.**, **Perir, A.** and **Vermeesch, P.** (2015) Physical controls on sand composition and relative durability of detrital minerals during ultra-long distance littoral and aeolian transport (Namibia and southern Angola). *Sedimentology*, **62**, 971–996.

Gehrels, G.E. (2014) Detrital zircon U-Pb geochronology applied to tectonics. *Annu. Rev. Earth Planet. Sci.*, **42**, 127–149.

Goudie, A.S. (2005) The drainage of Africa since the Cretaceous. *Geomorphology*, **67**, 437–456.

Gresse, P.G., **von Veh, M.W.** and **Frimmel, H.E.** (2006) Namibian (Neoproterozoic) to early Cambrian successions. In: *The Geology of South Africa* (Eds Johnson, M.R., Anhaeusser, C.R. and Thomas, R.J.), *Geol. Soc. S. Afr.*, 395–420.

Griffin, W.L., **Pearson, N.J.**, **Belousova, E.**, **Jackson, S.E.**, **van Achterbergh, E.**, **O'Reilly, S.Y.** and **Shee, S.R.** (2000) The Hf isotope composition of cratonic mantle: LAM-MCICPMS analysis of zircon megacrysts in kimberlites. *Geochim. Cosmochim. Acta*, **64**, 133–147.

Griffin, W.L., **Powell, W.J.**, **Pearson, N.J.** and **O'Reilly, S.Y.** (2008) Glitter: data reduction software for laser ablation

ICPMS. In: *Laser Ablation ICP-MS in the Earth Sciences: Current Practices and Outstanding Issues* (Ed. Sylvester, P.), *Min. Ass. Canada Short Course Ser.*, **40**, 308–311.

Gumsley, A.P., **Chamberlain, K.R.**, **Bleeker, W.**, **Söderlund, U.**, **de Kock, M.O.**, **Larsson, E.R.** and **Bekker, A.** (2017) Timing and tempo of the Great Oxidation Event. *Proc. Natl Acad. Sci. USA*, **114**, 1811–1816.

Haddon, I.G. (2005) *The sub-Kalahari geology and tectonic evolution of the Kalahari Basin, southern Africa*. PhD thesis, University of the Witwatersrand, Johannesburg, South Africa, 343 pp.

Haile, B.G., **Line, L.H.**, **Klausen, T.G.**, **Olaussen, S.**, **Eide, C.H.**, **Jahren, J.** and **Hellevang, H.** (2021) Quartz overgrowth textures and fluid inclusion hermometry evidence for basin-scale sedimentary recycling: an example from the Mesozoic Barents Sea Basin. *Basin Res.*, **33**, 1697–1710.

Hall, E.S., **Hitzman, M.W.**, **Kuiper, Y.D.**, **Kylander-Clark, A.R.C.**, **Holm-Denoma, C.S.**, **Moscati, R.J.**, **Plink-Björklund, P.** and **Enders, M.S.** (2018) Igneous and detrital zircon U-Pb and Lu-Hf geochronology of the late Meso- to Neoproterozoic northwest Botswana rift: Maximum depositional age and provenance of the Ghanzi Group, Kalahari Copperbelt, Botswana and Namibia. *Precambrian Res.*, **318**, 133–155.

Heilimo, E., **Halla, J.** and **Huhma, H.** (2011) Single-grain zircon U-Pb age constraints of the western and eastern sanukitoid zones in the Finnish part of the Karelian Province. *Lithos*, **121**, 87–99.

Heine, K. (1982) The main stages of the Late Quaternary evolution of the Kalahari Region, southern Africa. *Palaeoecol. Afr.*, **15**, 53–76.

Heinonen, A.P., **Andersen, T.** and **Rämö, O.T.** (2010) Source constraints from the Hf isotope composition of zircon in the rapakivi granites and associated mafic rocks of southern Finland. *J. Petrol.*, **51**, 1687–1709.

Hofmann, M., **Linnemann, U.**, **Hoffmann, K.-H.**, **Gerdes, A.**, **Eckelmann, K.** and **Gärtner, A.** (2014) The Namuskluft and Dreigratberg sections in southern Namibia (Kalahari craton, Gariep Belt): a geological history of Neoproterozoic rifting and recycling of cratonic crust during the dispersal of Rodinia until the amalgamation of Gondwana. *Int. J. Earth Sci.*, **103**, 1187–1202.

Hofmann, M., **Linnemann, U.**, **Hoffmann, K.-H.**, **Germs, G.**, **Gerdes, A.**, **Marko, L.**, **Eckelmann, K.**, **Gärtner, A.** and **Krause, R.** (2015) The four Neoproterozoic glaciations of southern Namibia and their detrital zircon record: the fingerprints of four crustal growth events during two supercontinent cycles. *Precambrian Res.*, **259**, 176–188.

Iizuka, T., **Campbell, I.H.**, **Allen, C.M.**, **Gill, J.B.**, **Maruyama, S.** and **Makoka, F.** (2013) Evolution of the African continental crust as recorded by U-Pb, Lu–Hf and O isotopes in detrital zircons from modern rivers. *Geochim. Cosmochim. Acta*, **107**, 96–120.

Iizuka, T., **Komiya, T.**, **Rino, S.**, **Maruyama, S.** and **Hirata, T.** (2010) Detrital zircon evidence for Hf isotopic evolution of granitic crust and continental growth. *Geochim. Cosmochim. Acta*, **74**, 2450–2472.

Jacobs, J., **Opås, B.**, **Elburg, M.A.**, **Läufer, A.**, **Estrada, S.**, **Ksienzyk, A.K.**, **Damaske, D.** and **Hofmann, M.** (2017) Cryptic sub-ice geology revealed by a U-Pb zircon study of glacial till in Dronning Maud Land, East Antarctica. *Precambrian Res.*, **294**, 1–14.

Johnson, M.R., **van Vuuren, C.J.**, **Visser, J.N.J.**, **Wickens, H.V.**, **Christie, A.D.M.**, **Roberts, D.L.** and **Brandl, G.** (2006) Sedimentary rocks of the Karoo Supergroup. In: *The Geology of South Africa* (Eds Johnson, M.R., Anhaeusser, C.R. and Thomas, R.J.), *Geol. Soc. S. Afr.*, 461–499.

Johnson, S.P., **Kirkland, C.L.**, **Evans, N.J.**, **McDonald, B.J.** and **Cutten, H.N.** (2018) The complexity of sediment recycling as revealed by common Pb isotopes in K-feldspar. *Geosci. Front.*, **9**, 1515–1527.

Key, R., **Cotterill, F.P.D.** and **Moore, A.E.** (2015) The Zambezi River: an archive of tectonic events linked to the amalgamation and disruption of Gondwana and subsequent evolution of the African Plate. *S. Afr. J. Geol.*, **118**, 425–438.

Klama, K.O. (2008) U-Pb Geochronologie, Hf Isotopie und Spurenelementgeochemie detritischer Zirkone aus rezenten Sedimenten des Orange- und Vaal River Flusssystems in Südafrika. PhD Thesis, Johann Wolfgang Goethe-Universität, Frankfurt am Main, Germany, 105 pp. http://publikationen.ub.uni-frankfurt.de/frontdoor/index/index/year/2009/docId/6594

Knight, J. (2021) The late Quaternary stratigraphy of coastal dunes and associated deposits in southern Africa. *S. Afr. J. Geol.*, **124**, 995–1006.

Kounev, A., **Viola, G.**, **de Wit, M.-J.** and **Andreoli, M.** (2008) A mid Cretaceous paleo-Karoo River valley across the Knersvlakte plain (northwestern coast of South Africa): evidence from apatite fission track analysis. *S. Afr. J. Geol.*, **111**, 409–420.

Kruger, A.C., **Goliger, A.M.**, **Retief, J.V.** and **Sekele, S.** (2010) Strong wind climatic zones in South Africa. *Wind Struct.*, **13**, 37–55.

Lancaster, N. (1981) Palaeoenvironmental implications of fixed dune systems in southern Africa. *Palaeogeogr. Palaeoclimatol. Palaeoecol.*, **33**, 327–346.

Lancaster, N. (1982) Dunes on the Skeleton Coast, Namibia (South West Africa): geomorphology and grain size relationships. *Earth Surf. Process. Landf.*, **7**, 575–587.

Lancaster, N. and **Ollier, C.D.** (1983) Sources of sand for the Namib sand sea. *Zeitschrift Für Geomorphol. Sup.*, **45**, 71–83.

Ledent, D., **Patterson, C.** and **Tilton, G.** (1964) Ages of zircon and feldspar concentrates from North American beach and river sands. *J. Geol.*, **72**, 112–122.

Lynn, M.D. (1998) Diamonds. In: *The mineral resources of South Africa* (Eds Wilson, M.G.C. and Anhaeusser, C.R.), *Coun. Geosci. S. Afr.*, Handbook **16**, 232–258.

Mabbutt, J.A. (1977) *Desert Landforms*. Australian National University Press, Canberra, 340 pp.

Mapeo, R.B.M., **Armstrong, R.A.**, **Kampunzu, A.B.**, **Modisi, M.P.**, **Ramokate, L.V.** and **Modie, B.N.J.** (2006) A ca. 200Ma hiatus between the lower and Upper Transvaal Groups of southern Africa: SHRIMP U-Pb detrital zircon evidence from the Segwagwa Group, Botswana: implications for Palaeoproterozoic glaciations. *Earth Planet. Sci. Lett.*, **244**, 113–132.

Mapeo, R.B.M., **Ramokate, L.V.**, **Armstrong, R.A.** and **Kampunzu, A.B.** (2004) U-Pb zircon age of the upper Palapye group (Botswana) and regional implications. *J. Afr. Earth Sci.*, **40**, 1–16.

Master, S., **Bekker, A.** and **Hofmann, A.** (2010) A review of the stratigraphy and geological setting of the Palaeoproterozoic Magondi Supergroup, Zimbabwe – type locality for the Lomagundi carbon isotope excursion. *Precambrian Res.*, **182**, 254–273.

Matmon, A., **Hidy, A.J.**, **Vainer, S.**, **Crouvi, O.**, **Fink, D.**, **Erel, Y.**, **ASTER Team**, **Horwits, L.K.** and **Chazan, M.** (2015) New chronology for the southern Kalahari Group

sediments with implications for sediment-cycle dynamics and early hominim occupation. *Quatern. Res.*, **84**, 118–132.

McCarthy, T.S. (1983) Evidence for the former existence of a major, southerly flowing river in Griqualand West. *Trans. Geol. Soc. S. Afr.*, **86**, 37–49.

Meert, J.C. (2014) Strange attractors, spiritual interlopers and lonely wanderers: the search for pre-Pangean supercontinents. *Geosci. Front.*, **5**, 155–166.

Milani, E.J. and **de Wit, M.J.** (2008) Correlations between the classic Paraná and Cape-Karoo sequences of South America and southern Africa and their basin infills flanking the Gondwanides: du Toit revisited. *Geol. Soc. Lond. Spec. Publ.*, **394**, 319–342.

Miller, R.M. (2014) Evidence for the evolution of the Kalahari dunes from the Auob River, southeastern Namibia. *Trans. Roy. Soc. S. Afr.*, **69**, 195–204.

Modie, B.N. (2000) Geology and mineralization in the Meso- to Neoproterozoic Ghanzi-Chobe Belt of northwest Botswana. *J. Afr. Earth Sci.*, **30**, 467–474.

Moore, A.E. (1999) A reappraisal of epeirogenic flexure axes in southern Africa. *S. Afr. J. Geol.*, **102**, 363–376.

Moore, A.E., **Cotterill, F.P.D.** and **Eckardt, F.D.** (2012a) The evolution and ages of Makgadikgadi palaeo-lakes: consilient evidence from Kalahari drainage evolution south-central Africa. *S. Afr. J. Geol.*, **115**, 385–413.

Moore, J.M. and **Moore, A.E.** (2004) The roles of primary kimberlitic and secondary Dwyka glacial sources in the development of alluvial and marine diamond deposits in Southern Africa. *J. Afr. Earth Sci.*, **38**, 115–134.

Moore, J.M., **Polteau, S.**, **Armstrong, R.A.**, **Corfu, F.** and **Tsikos, H.** (2012b) The age and correlation of the Postmasburg Group, southern Africa: constraints from detrital zircon grains. *J. Afr. Earth Sci.*, **64**, 9–19.

van Niekerk, H.S. and **Beukes, N.J.** (2019) Revised definition/outline of the Kheis Terrane along the western margin of the Kaapvaal Craton and lithostratigraphy of the newly proposed Keis Supergroup. *S. Afr. J. Geol*, **122**, 187–220.

van Niekerk, H.S., **Elburg, M.A.**, **Andersen, T.** and **Armstrong, R.A.** (2022) Provenance of metasedimentary rocks of the Kheis Terrane and Kakamas Domain: support for accretionary tectonics during the development of the western Namaqua-Natal metamorphic province. *S. Afr. J. Geol.*, **125**, 61–78.

Partridge, T.C., **Botha, G.A.** and **Haddon, I.G.** (2006) Cenozoic deposits of the interior. In: *The Geology of South Africa* (Eds Johnson, M.R., Anhaeusser, C.R. and Thomas, R.J.), *Geol. Soc. S. Afr.*, 585–604.

Partridge, T.C. and **Maud, R.R.** (1987) Geomorphic evolution of southern Africa since the Mesozoic. *S. Afr. J. Geol.*, **90**, 179–208.

Pettijohn, F.J., **Potter, P.E.** and **Siever, R.** (1973) *Sand and Sandstone*. Springer Verlag, Berlin, Heidelberg, 618 pp.

Philander, C. and **Rozendaal, A.** (2015) Detrital zircon geochemistry and U-Pb geochronology as an indicator of provenance of the Namakwa Sands heavy mineral deposit, west coast of South Africa. *Sed. Geol.*, **328**, 1–16.

Potter, P.E. and **Pryor, W.A.** (1961) Dispersal Centers of Paleozoic and later clastics of the Upper Mississippi Valley and adjacent areas. *Geol. Soc. Am. Bull.*, **72**, 1195–1250.

Prave, A.R., **Hoffmann, K.-H.**, **Hegenberger, W.** and **Fallick, A.E.** (2011) The Witvlei Group of East-Central Namibia. In: *The Geological Record of Neoproterozoic Glaciations* (Eds Arnaud, E., Halverson, G.P. and Shields-Zhou, G.), *Geol. Soc, Lond. Mem.*, **36**, 211–216.

Pye, K. and **Tsoar, H.** (2009) *Aeolian Sand and Sand Dunes*. Springer-Verlag, Berlin, Heidelberg, 458 pp.

Ramokate, L.V., **Mapeo, R.B.M.**, **Corfu, F.** and **Kampunzu, A.B.** (2000) Proterozoic geology and regional correlation of the Ghanzi-Makunda area, western Botswana. *J. Afr. Earth Sci.*, **30**, 453–466.

Reinhard, C.T., **Planavsky, N.J.** and **Lyons, T.W.** (2013) Long-term sedimentary recycling of rare sulphur isotope anomalies. *Nature*, **497**, 100–103.

Roberts, D., **Cawthra, H.** and **Musekiva, C.** (2013) Dynamics of late Cenozoic aeolian deposition along the South African coast: a record of evolving climate and ecosystems. In: *Sedimentary Coastal Zones from High to Low Latitudes* (Eds Martini, I.P. and Wanless, H.R.), *Geol. Soc., Lond. Spec. Publ.*, **388**, 353–387.

Røhr, T.S., **Andersen, T.** and **Dypvik, H.** (2008) Provenance of lower cretaceous sediments in the Wandel Sea Basin, North Greenland. *J. Geol. Soc.*, **165**, 755–767.

Røhr, T.S., **Andersen, T.**, **Dypvik, H.** and **Embry, A.F.** (2010) Detrital zircon characteristics of the Lower Cretaceous Isachsen Formation, Sverdrup Basin; source constraints from age and Hf isotope data. *Can. J. Earth Sci.*, **47**, 255–271.

Rubidge, B.S., **Erwin, D.H.**, **Ramezani, J.**, **Bowring, S.** and **de Klerk, W.J.** (2013) High-precision temporal calibration of Late Permian vertebrate biostratigraphy: U-Pb zircon constraints from the Karoo Supergroup, South Africa. *Geology*, **41**, 363–366.

van Schijndel, V., **Cornell, D.H.**, **Hoffmann, K.-H.** and **Frei, D.** (2011) Three episodes of crustal development in the Rehoboth Province, Namibia. *Geol. Soc. Lond. Spec. Publ.*, **357**, 27–47.

van Schijndel, V., **Cornell, D.H.**, **Frei, D.**, **Simonsen, S.L.** and **Whitehouse, M.J.** (2014) Crustal evolution of the Rehoboth Province from Archaean to Mesoproterozoic times: insights from the Rehoboth Basement Inlier. *Precambrian Res.*, **240**, 22–36.

Schlüter, T. (2006) *Geological Atlas of Africa*. Springer-Verlag, Berlin, Heidelberg, 272 pp.

Schröder, S., **Beukes, N.J.** and **Armstrong, R.A.** (2016) Detrital zircon constraints on the tectonostratigraphy of the Paleoproterozoic Pretoria Group, South Africa. *Precambrian Res.*, **278**, 362–393.

da Silva, R. (2011) Distribution and geochronology of unconformity-bound sequences in Palaeoproterozoic Elim-Olifantshoek red beds: Implications for timing and formation of Sishen-type iron ore a heavy carbonate carbon isotope excursions. MSc thesis, University of Johannesburg, South Africa, 110 pp.

Söderlund, U., **Patchett, J.P.**, **Vervoort, J.D.** and **Isachsen, C.E.** (2004) The ^{176}Lu decay constant determined by Lu-Hf and U-Pb isotope systematics of Precambrian mafic intrusions. *Earth Planet. Sci. Lett.*, **219**, 311–324.

Stacey, J.S. and **Kramers, J.D.** (1975) Approximation of terrestrial lead isotope evolution by a two-stage model. *Earth Planet. Sci. Lett.*, **26**, 207–221.

Stone, A. (2021) Dryland dunes and other dryland environmental archives as proxies for Late Quaternary stratigraphy and environmental and climate change in southern Africa. *S. Afr. J. Geol.*, **124**, 927–962.

Strobach, B.J. (2008) Mapping the major catchments of Namibia. *Agricola*, **2008**, 63–73.

Tatsumoto, M. and **Patterson, C.** (1964) Age studies of zircon and feldspar concentrates from the Franconia sandstone. *J. Geol.*, **72**, 232–242.

Telfer, M.W. and **Thomas, D.S.G.** (2007) Late Quaternary linear dune accumulation and chronostratigraphy of the southwestern Kalahari: implications for aeolian palaeoclimatic reconstructions and predictions of future dynamics. *Quatern. Sci. Rev.*, **26**, 2617–2630.

Thamm, A.G. and **Johnson, M.R.** (2006) The Cape Supergroup. In: *The Geology of South Africa* (Eds Johnson, M.R., Anhaeusser, C.R. and Thomas, R.J.), *Geol. Soc. S. Afr.*, 443–460.

Thomas, D.S.G. and **Burrough, S.L.** (2016) Luminescence-based dune chronologies in southern Africa: analysis and interpretation of dune database records across the subcontinent. *Quatern. Int.*, **410**, 30–45.

Thomas, D.S.G. and **Shaw, P.A.** (1991) *The Kalahari Environment*. Cambridge University Press, Cambridge, 284 pp.

Vainer, S., **Erel, Y.** and **Matmon, A.** (2018) Provenance and depositional environments of Quaternary sediments in the southern Kalahari Basin. *Chem. Geol.*, **476**, 352–369.

Veizer, J. and **Jansen, S.L.** (1979) Basement and sedimentary recycling and continental evolution. *J. Geol.*, **87**, 341–370.

Vickers-Rich, P., **Narbonne, G.**, **Laflamme, M.**, **Darroch, S.**, **Kaufman, A.**, **Kriesfeld, L.**, **Hall, M.**, **Trusler, P.**, **Smith, J.**, **Elliot, D.**, **Ivantsov, A.**, **Fedonkin, M.**, **Schneider, G.**, **Hoffmann, C.**, **Hinder, G.**, **Boehm-Erni, B.**, **Roemer, B.** and **von Schumann, G.** (2016) The Nama Group of southern Namibia. The end game of the first large, complex organisms on earth, the Ediacarans [IGCP493/587]. 35th International Geological Congress, 2016 Pre-conference field guide. https://www.monash.edu/__data/assets/pdf_file/0007/756286/35th-International-Geological-Congress-2nd-ed.pdf

Visser, J.N.J. (1987) The palaeogeography of part of southwestern Gondwana during the Permo-Carboniferous glaciation. *Palaeogeogr. Palaeoclimatol. Palaeoecol.*, **61**, 205–219.

Watkeys, M.K. (2006) Gondwana break-up: a South African perspective. In: *The Geology of South Africa* (Eds Johnson, M.R., Anhaeusser, C.R. and Thomas, R.J.), *Geol. Soc. S. Afr.*, 531–539.

Williams, I.E. (2001) Response of detrital zircon and monazite, and their U-Pbisotopic systems, to regional metamorphism and host-rock partial melting, Cooma Complex, southeastern Australia. *Aust. J. Earth Sci.*, **48**, 557–580.

de Wit, M.C.J. (1999) Post-Gondwana drainage and the development of diamond placers in western South Africa. *Econ. Geol.*, **94**, 721–740.

Woodhead, J.D. and **Hergt, J.M.** (2005) A preliminary appraisal of seven natural zircon reference materials for in situ Hf isotope determination. *Geostand. Geoanal. Re.*, **29**, 183–195.

Zeh, A., **Ovtcharova, M.**, **Wilson, A.H.** and **Schaltegger, U.** (2015) The Bushveld Complex was emplaced and cooled in less than one million years – results of zirconology, and geotectonic implications. *Earth Planet. Sci. Lett.*, **418**, 103–114.

Zeh, A., **Wilson, A.H.** and **Ovtcharova, M.** (2016) Source and age of upper Transvaal Supergroup, South Africa: age-Hf isotope record of zircons in Magaliesberg quartzite and Dullstroom lava, and implications for Paleoproterozoic (2.5–2.0 Ga) continent reconstruction. *Precambrian Res.*, **278**, 1–21.

Zeh, A., **Wilson, A.H.** and **Gerdes, A.** (2020) Zircon U-Pb-Hf isotope systematics of Transvaal Supergroup – constraints for the geodynamic evolution of the Kaapvaal Craton and its hinterland between 2.65 and 2.06 Ga. *Precambrian Res.*, **345**, 105760.

Zieger, J., **Rothe, J.**, **Hofmann, M.**, **Gärtner, A.** and **Linnemann, U.** (2019) The Permo-Carboniferous Dwyka Group of the Aranos Basin (Namibia) –how detrital zircons help understanding sedimentary recycling during a major glaciation. *J. Afr. Earth Sci.*, **158**, 103555.

Zieger, J., **Stutzriemer, M.**, **Hofmann, M.**, **Gärtner, A.**, **Gerdes, A.**, **Marko, L.** and **Linnemann, U.** (2021) The evolution of the southern Namibian Karoo-aged basins: implications from detrital zircon geochronologic and geochemistry data. *Int. Geol. Rev.*, **63**, 1758–1781.

Zimmermann, U. (2018) The provenance of selected Neoproterozoic to lower Paleozoic basin successions of Southwest Gondwana: a review and proposal for further research. In: *Geology of Southwest Gondwana* (Eds Siegesmund, S., Basei, M.A.S., Oyhantcabal, P. and Oriolo, S.), *Reg. Geol. Rev.*, 561-591. Springer International Publishing AG.

Manuscript received 16 September 2021; revision 16 March 2022; revision accepted 29 March 2022

Supporting Information

Additional information may be found in the online version of this article:

Table S1. U-Pb and Lu-Hf data of detrital zircon.